Author/s:
Zaib, S;Younas, MT;Khan, I;Ali, HS;McAdam, CJ;White, JM;Jaber, F;Awwad, NS;Ibrahium, HA

Title:
Pyrimidine-morpholine hybrids as potent druggable therapeutics for Alzheimer's disease: Synthesis, biochemical and in silico analyses

Date:
2023-12-01

Citation:
Zaib, S., Younas, M. T., Khan, I., Ali, H. S., McAdam, C. J., White, J. M., Jaber, F., Awwad, N. S. & Ibrahium, H. A. (2023). Pyrimidine-morpholine hybrids as potent druggable therapeutics for Alzheimer's disease: Synthesis, biochemical and in silico analyses. Bioorganic Chemistry, 141, https://doi.org/10.1016/j.bioorg.2023.106868.

Persistent Link:
https://hdl.handle.net/11343/337214

Bioorganic Chemistry 141 (2023) 106868

Contents lists available at ScienceDirect

Bioorganic Chemistry

journal homepage: www.elsevier.com/locate/bioorg

Pyrimidine-morpholine hybrids as potent druggable therapeutics for Alzheimer's disease: Synthesis, biochemical and in silico analyses

Sumera Zaib [a,*], Muhammad Tayyab Younas [a], Imtiaz Khan [b,*], Hafiz Saqib Ali [c], Christopher John McAdam [d], Jonathan M. White [e], Fadi Jaber [f,g], Nasser S. Awwad [h], Hala A. Ibrahium [i]

[a] Department of Basic and Applied Chemistry, Faculty of Science and Technology, University of Central Punjab, Lahore 54590, Pakistan
[b] Department of Chemistry and Manchester Institute of Biotechnology, The University of Manchester, 131 Princess Street, Manchester MI 7DN, UK
[c] Chemistry Research Laboratory, Department of Chemistry and the INEOS Oxford Institute for Antimicrobial Research, University of Oxford, 12 Mansfield Road, Oxford OX1 3TA, UK
[d] Department of Chemistry, University of Otago, P.O. Box 56, Dunedin 9054, New Zealand
[e] School of Chemistry and Bio-21 Institute, University of Melbourne, 3052 Parkville, Australia
[f] Department of Biomedical Engineering, Ajman University, Ajman, United Arab Emirates
[g] Center of Medical and Bio-Allied Health Sciences Research, Ajman University, Ajman, United Arab Emirates
[h] Department of Chemistry, King Khalid University, P.O. Box 9004, Abha 61413, Saudi Arabia
[i] Biology Department, Faculty of Science, King Khalid University, P.O. Box 9004, Abha 61413, Saudi Arabia

ARTICLE INFO

Keywords:
Alzheimer's disease
Cholinesterases
Enzyme assays
MD simulation
Morpholine
Palladium catalysis
Pyrimidine
Suzuki coupling

ABSTRACT

The identification of effective and druggable cholinesterase inhibitors to treat progressive neurodegenerative Alzheimer's disorder remains a continuous drug discovery hunt. In this perspective, the present study investigates the design and discovery of pyrimidine-morpholine hybrids (**5a-l**) as potent cholinesterase inhibitors. Palladium-catalyzed Suzuki-Miyaura cross-coupling reaction was employed to introduce the structural diversity on the pyrimidine heterocyclic core. A range of commercially available boronic acids was successfully coupled showing a high functional group tolerance. *In vitro* cholinesterase inhibitory potential using Ellman's method revealed significantly strong potency. Compound **5h** bearing a *meta*-tolyl substituent at 2-position of pyrimidine ring emerged as a lead candidate against AChE with an inhibitory potency of 0.43 ± 0.42 μM, ~38-fold stronger value than neostigmine (IC_{50} = 16.3 ± 1.12 μM). Compound **5h** also showed the lead inhibition against BuChE with an IC_{50} value of 2.5 ± 0.04 μM. The kinetics analysis of **5h** revealed the non-competitive mode of inhibition against AChE whereas computational modelling results of potent leads depicted diverse contacts with the binding site amino acid residues. Molecular dynamics simulations revealed the stability of biomolecular system, while, ADME analysis demonstrated druglikeness behaviour of potent compounds. Overall, the investigated pyrimidine-morpholine scaffold presented a remarkable potential to be developed as efficacious anti-Alzheimer's drugs.

1. Introduction

Alzheimer's disease (AD) is a chronic neurological disorder that influence many parts of the body including central nervous system. It is the most common forms of dementia and progressive neurodegenerative disorder with memory loss, cognitive decline, and language dysfunction in people above the age of 60 [1]. Patients with mild cognitive impairment (MCI) are at increased risk of progression to Alzheimer's, however, there are currently no effective drugs to treat this diseases. Several potential hypotheses have been proposed for the development of AD, however, the exact pathogenesis and etiology of this disease remain unclear [2]. Several factors are believed to contribute to the progression of the AD and the cholinergic deficit indicating the low levels of acetylcholine (ACh) remains prominent [3]. Acetylcholine is a neurotransmitter that plays a role in memory, learning, attention, and involuntary muscle movement and is hydrolyzed into acetate and choline by acetylcholinesterase (AChE) and butyrylcholinesterase (BuChE) [4]. AChE is primarily present in the central nervous system (CNS) while BuChE is found in the neurons. As AChE plays the leading role in the hydrolysis of ACh at a different stages of AD [5], the development of

* Corresponding authors.
E-mail addresses: sumera.zaib@ucp.edu.pk (S. Zaib), kimtiaz@hotmail.co.uk (I. Khan).

https://doi.org/10.1016/j.bioorg.2023.106868
Received 12 July 2023; Received in revised form 2 September 2023; Accepted 15 September 2023
Available online 16 September 2023

novel inhibitors of AChE that can enhance the cholinergic neurotransmission and reduce acetylcholine hydrolysis, is considered as a promising strategy to combat AD [6–8]. Recent literature reports have documented several classes of compounds with cholinesterase inhibitory potential [9–13]. Moreover, the commercially available and approved AChE inhibitors including donepezil, rivastigmine, tacrine, galantamine and huperzine A enhance ACh levels at synapses, thus improving the neurotransmission. However, severe side effects of these drugs, including nausea, vomiting, decreased appetite, weight loss, and liver toxicity [14–16] demand the drug discovery community to explore wider chemical space and identify potent and efficacious anticholinesterase agents to manage AD more effectively.

Nitrogen-containing heterocycles are among the top structural pharmacophores contributing enormously towards the generation of bioactive pharmaceuticals. A recently compiled databank of U.S. FDA approved pharmaceutical drugs revealed that nitrogen heterocycles are present in 59% of small-molecule drugs [17]. Among them, pyrimidine nucleus remains at the forefront of drug discovery efforts in achieving the drug molecules targeting various targets. A plethora of commercial drugs/drug candidates containing a pyrimidine scaffold continues to grow and significant interest of medicinal chemistry community makes this heterocycle a valuable entity to be explored. Pyrimidine derivatives exhibit a diverse range of biological functions including anticancer, antiviral, antimicrobial, anti-inflammatory, antimalarial, antihypertensive, anticonvulsant, antitubercular, antioxidant and analgesic activities [18–21]. The incorporation of pyrimidine ring in various FDA approved drugs provides a promising impetus to explore the wider chemical space to deliver new drugs.

In parallel, morpholine heterocycle is also a predominant entity of numerous FDA approved and experimental drugs. It is widely accepted as a useful scaffold in drug discovery arena due to its promising physicochemical, metabolic and biological properties [22]. Morpholine scaffold also presents a wide range of biological potential including anticancer, anti-inflammatory, antiviral, antihyperlipidemic, analgesic, antioxidant, antipyretic, antimicrobial, antiobesity, antileishmanial and antineurodegenerative activities [23–27]. Morpholine containing compounds have targeted a range of enzymes such as kinases, squalene synthase, amyloid β (Aβ) peptides, γ-secretase, cholinesterases, monoamine oxidases, Factor Xa, autotaxin, nuclear factor erythroid 2-related factor 2, topoisomerases, peptidyl transferase, ribonucleotide reductase, α-glucosidase [22]. Therefore, in view of the great interest in the medicinal chemistry of morpholine nucleus, the exploration of biological profile against different targets remains a burgeoning theme of research. Fig. 1 demonstrates the medicinal potential of pyrimidine and morpholine scaffolds and rationale of our approach towards the design of anti-Alzheimer's agents.

Over the last few decades, transition-metal-catalyzed cross-coupling methods (Suzuki-Miyaura, Heck, Sonogashira, Hiyama, Stille, Negishi, Kumada) have become fundamental reactions in modern (bio)organic chemistry and industrial settings to generate new carbon–carbon bonds [28–32]. Among these methods, palladium-catalyzed Suzuki-Miyaura reaction represents the cross-coupling of two sp^2-centers involving an electrophilic and a nucleophilic partner, thus enabling a revolutionary approach to access biaryl frameworks [33–41]. Moreover, easy accessibility and commercial availability of starting precursors, high functional group tolerance and air/moisture tolerant properties make this method an indispensable tool in the organic chemist's arsenal [42,43]. The industrial application of Suzuki-Miyaura cross-coupling reaction has been well-realized in the production of several drugs and pharmaceutical fragments including Losartan (angiotensin II receptor antagonist), Etalocib (anti-cancer), Boscalid (fungicide), OSU-6162 (dopamine stabilizer), LY503430 (anti-Parkinson's), LY451395 (anti-Alzheimer's), PDE4 inhibitor (anti-COPD) [42,44–48].

Despite the development of structurally diverse nitrogen-containing heterocyclic entities as drug pharmacophores, the development of new strategies and innovative solutions enabling the improved and speedy production of target drug molecules is highly desirable to meet the enormous pressure of selective drug scarcity. In this perspective and building on our continuous curiosity in the development of cholinesterase inhibitors [49–56], current synthetic chemistry efforts were envisioned exploring impactful heterocyclic entities (pyrimidine and morpholine) endowed with a diverse substitution pattern to expand the drug discovery arena. In line with medicinal chemistry protocols, robust, reliable and quick chemical transformation to achieve varied pendent functionalities on the heterocyclic ring, Suzuki-Miyaura cross-coupling reaction was employed. A diverse selection of boronic acids was used to introduce the structural diversity to pyrimidine ring. *In vitro* anticholinesterase inhibitory data identified various significantly potent inhibitors while kinetics studies of the lead molecule revealed the non-competitive inhibition of AChE. *In silico* docking analysis shed light on the binding modes of the potent inhibitors which showed multiple contacts with the active site amino acids of cholinesterases. Finally, ADME analysis showed promising druglike properties suggesting that the designed molecules could be considered as a prototype for the development of lead inhibitors to treat AD.

2. Materials and methods

2.1. Experimental and characterization data

2.1.1. Synthesis of 4-(2-chloropyrimidin-4-yl)morpholine (3)

Morpholine (1.1 equiv) was added dropwise to a cooled solution of 2,4-dichloropyrimidine (1 equiv), and *N*,*N*-diisopropylethylamine (DIPEA) (1.3 equiv) in IPA (3 mL/mmol) at 0 °C. The reaction mixture was warmed to room temperature (RT) and stirred for 12 h. After completion (TLC, 100% EtOAc), the volatiles were evaporated and resulting residue was taken up in EtOAc. After washing with water, the organic phase was dried ($MgSO_4$), filtered and evaporated under reduced pressure. The purification by silica column chromatography (eluent = 30 → 60% EtOAc in hexanes) afforded compound **3** as a white solid (844 mg) in 82% yield [57]. R_f = 0.63 (eluent = 100% EtOAc); FTIR ν_{max}/cm^{-1} (film) 3081, 2990, 1657, 1598, 1190, 1030, 761; ^1H NMR (400 MHz, $CDCl_3$) δ_H: 8.05 (d, J = 6.2 Hz, 1H), 6.38 (d, J = 6.2 Hz, 1H), 3.78–3.72 (m, 4H), 3.69–3.55 (m, 4H); $^{13}C\{^1H\}$ NMR (101 MHz, $CDCl_3$) δ_C: 162.9, 160.7, 157.4, 101.2, 66.4, 44.4.

2.1.2. Palladium-catalyzed Suzuki coupling

To an appropriate reaction vessel containing a magnetic follower was charged with 4-(2-chloropyrimidin-4-yl)morpholine (0.25 mmol, 1.0 equiv), boronic acid/ester (0.30 mmol, 1.2 equiv), $Pd(dppf)Cl_2$ (0.025 mmol, 10 mol%) and 2 M aqueous potassium carbonate (0.625 mmol, 2.5 equiv), in a mixture of toluene and ethanol (2:1, 5 mL). The reaction mixture was sparged with N_2 for 5 min before heating to 80 °C and stirring for 12 h. After cooling to RT, EtOAc (10 mL) was added to the reaction mixture and passed through a short pad of celite. The filtrate was washed with water (2 × 10 mL) and organic phase was dried ($MgSO_4$) and filtered. The solvent was removed *in vacuo* and the residue was purified by silica column chromatography (eluent = 20 → 80% EtOAc in hexanes) to afford compounds **5a-l**.

*2.1.2.1. 4-(2-Phenylpyrimidin-4-yl)morpholine (**5a**).* Colorless oil (58 mg, 97% yield). R_f = 0.63 (eluent = 100% EtOAc); FTIR ν_{max} / cm^{-1} (film) 3044, 2988, 1665, 1609, 1197, 1043; ^1H NMR (400 MHz, $CDCl_3$) δ_H: 8.42–8.36 (m, 2H), 8.34 (d, J = 6.2 Hz, 1H), 7.50–7.42 (m, J = 6.7, 3.5 Hz, 3H), 6.40 (d, J = 6.2 Hz, 1H), 3.85–3.77 (m, 4H), 3.76–3.67 (m, 4H); $^{13}C\{^1H\}$NMR (101 MHz, $CDCl_3$) δ_C: 163.5, 162.0, 155.7, 137.9, 130.6, 128.5, 128.2, 100.9, 66.6, 44.2; Anal. calcd. for $C_{14}H_{15}N_3O$ (241.12): C, 69.69; H, 6.27; N, 17.41%; found: C, 69.60; H, 6.17; N, 17.33%.

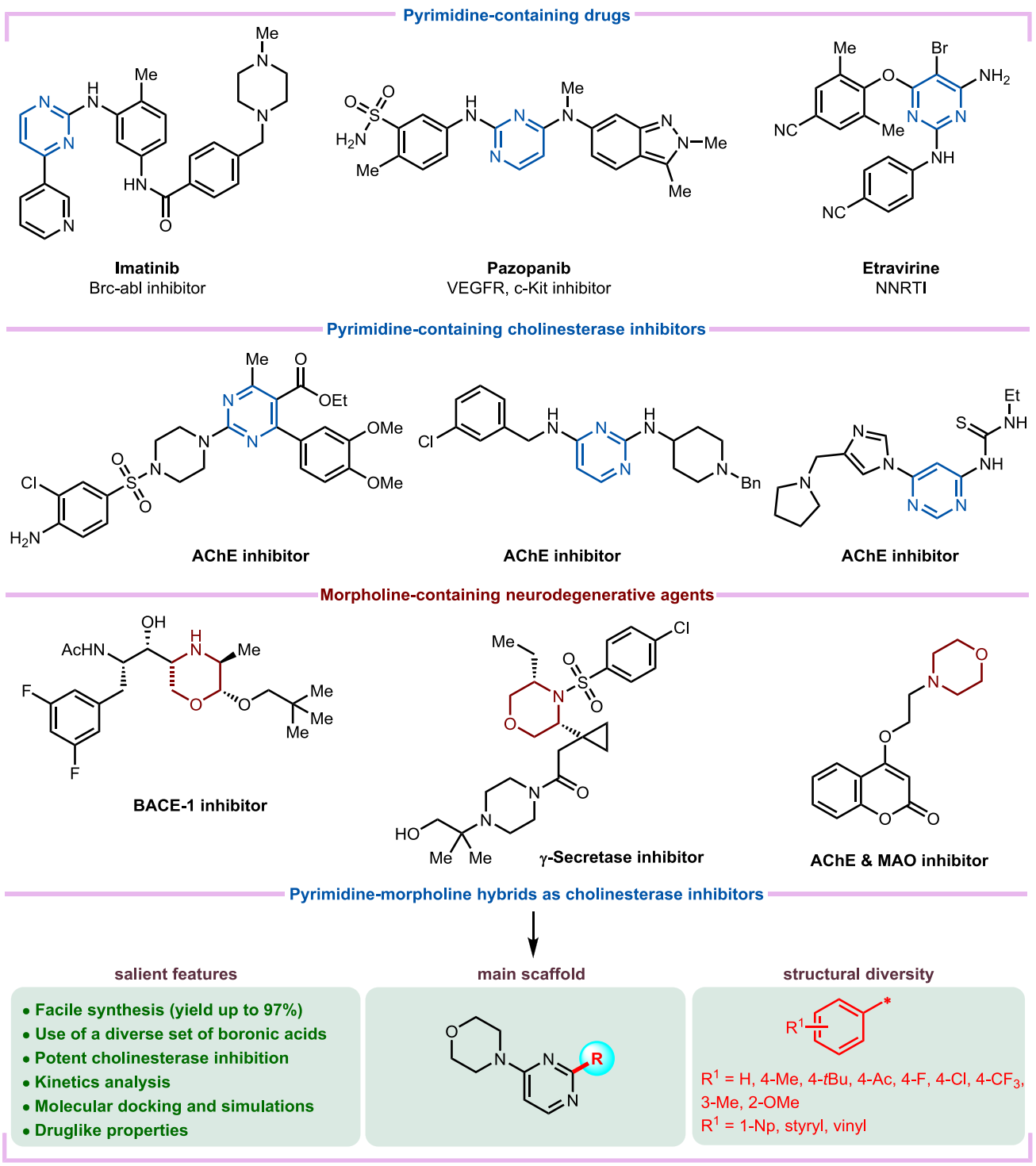

Fig. 1. Medicinal potential of pyrimidine and morpholine scaffolds and rationale of our approach.

*2.1.2.2. 4-(2-(p-Tolyl)pyrimidin-4-yl)morpholine (**5b**).* Off-white solid (59 mg, 93% yield). $R_f = 0.60$ (eluent = 100% EtOAc); FTIR ν_{max} / cm^{-1} (film) 3048, 2981, 1660, 1623, 1205, 1036; ^1H NMR (400 MHz, $CDCl_3$) δ_H: 8.34 (d, $J = 6.2$ Hz, 1H), 8.30 (d, $J = 8.2$ Hz, 2H), 7.27 (d, $J = 8.1$ Hz, 2H), 6.39 (d, $J = 6.2$ Hz, 1H), 3.85–3.78 (m, 4H), 3.77–3.68 (m, 4H), 2.42 (s, 3H); $^{13}C\{^1H\}$NMR (101 MHz, $CDCl_3$) δ_C: 163.5, 162.0, 155.7, 140.8, 135.2, 129.2, 128.1, 100.7, 66.6, 44.2, 21.6; Anal. calcd. for $C_{15}H_{17}N_3O$ (255.14): C, 70.56; H, 6.71; N, 16.46%; found: C, 70.50; H, 6.73; N, 16.39%.

*2.1.2.3. 4-(2-(4-(tert-Butyl)phenyl)pyrimidin-4-yl)morpholine (**5c**).* Off-white solid (41 mg, 55% yield). $R_f = 0.57$ (eluent = 100% EtOAc); FTIR ν_{max} / cm^{-1} (film) 3065, 2975, 1678, 1620, 1169, 1036; ^1H NMR (400 MHz, $CDCl_3$) δ_H: 8.34 (d, $J = 6.2$ Hz, 1H), 8.30 (d, $J = 8.5$ Hz, 2H), 7.48 (d, $J = 8.5$ Hz, 2H), 6.39 (d, $J = 6.2$ Hz, 1H), 3.86–3.78 (m, 4H), 3.76–3.69 (m, 4H), 1.35 (s, 9H); $^{13}C\{^1H\}$NMR (101 MHz, $CDCl_3$) δ_C: 163.5, 162.0, 155.7, 154.0, 135.1, 128.0, 125.4, 100.7, 66.7, 44.2, 34.9, 31.4; Anal. calcd. for $C_{18}H_{23}N_3O$ (297.18): C, 72.70; H, 7.80; N, 14.13%; found: C, 72.63; H, 7.84; N, 14.05%.

*2.1.2.4. 1-(4-(4-Morpholinopyrimidin-2-yl)phenyl)ethan-1-one (**5d**).* Off-white solid (59 mg, 84% yield). $R_f = 0.43$ (eluent = 100% EtOAc); FTIR ν_{max} / cm^{-1} (film) 3055, 2980, 1712, 1659, 1599, 1163, 1029; ^1H NMR (400 MHz, $CDCl_3$) δ_H: 8.45 (d, $J = 8.5$ Hz, 2H), 8.36 (d, $J = 6.1$ Hz, 1H), 8.01 (d, $J = 8.5$ Hz, 2H), 6.44 (d, $J = 6.2$ Hz, 1H), 3.87–3.79 (m, 4H), 3.76–3.67 (m, 4H), 2.63 (s, 3H); $^{13}C\{^1H\}$NMR (101 MHz, $CDCl_3$) δ_C: 198.1, 162.7, 162.1, 156.3, 142.6, 138.3, 128.4, 128.3, 101.5, 66.6, 44.2, 26.9; Anal. calcd. for $C_{16}H_{17}N_3O_2$ (283.13): C, 67.83; H, 6.05; N, 14.83%; found: C, 67.78; H, 5.96; N, 14.88%.

*2.1.2.5. 4-(2-(4-Fluorophenyl)pyrimidin-4-yl)morpholine (**5e**).* Off-white solid (58 mg, 90% yield). $R_f = 0.61$ (eluent = 100% EtOAc); FTIR ν_{max} / cm^{-1} (film) 3041, 2990, 1662, 1614, 1188, 1056; ^1H NMR (400 MHz, $CDCl_3$) δ_H: 8.43–8.35 (m, 2H), 8.31 (d, $J = 5.1$ Hz, 1H), 7.15–7.07 (m, 2H), 6.40 (d, $J = 6.2$ Hz, 1H), 3.84–3.76 (m, 4H), 3.76–3.66 (m, 4H); $^{13}C\{^1H\}$NMR (101 MHz, $CDCl_3$) δ_C: 164.6 (d, $J = 251.5$ Hz), 162.5, 162.0, 155.6, 134.0 (d, $J = 3.0$ Hz), 130.3 (d, $J = 8.1$ Hz), 115.3 (d, $J = 21.2$ Hz), 100.8, 66.6, 44.2; $^{19}F\{^1H\}$NMR (376 Hz, $CDCl_3$) δ_F: $^-$110.7; Anal. calcd. for $C_{14}H_{14}FN_3O$ (259.11): C, 64.85; H, 5.44; N, 16.21%; found: C, 64.77; H, 5.32; N, 16.12%.

*2.1.2.6. 4-(2-(4-Chlorophenyl)pyrimidin-4-yl)morpholine (**5f**).* Off-white solid (44 mg, 73% yield). $R_f = 0.61$ (eluent = 100% EtOAc); FTIR ν_{max} / cm^{-1} (film) 3061, 2967, 1672, 1618, 1166, 1031; ^1H NMR (400 MHz, $CDCl_3$) δ_H: 8.33 (dd, $J = 7.4$, 0.9 Hz, 3H), 7.41 (d, $J = 8.6$ Hz, 2H), 6.41 (d, $J = 6.2$ Hz, 1H), 3.87–3.78 (m, 4H), 3.77–3.67 (m, 4H); $^{13}C\{^1H\}$NMR (101 MHz, $CDCl_3$) δ_C: 162.6, 162.0, 155.8, 136.7, 136.4, 129.6, 128.6, 101.1, 66.6, 44.2; Anal. calcd. for $C_{14}H_{14}ClN_3O$ (275.08): C, 60.98; H, 5.12; N, 15.24%; found: C, 60.87; H, 5.08; N, 15.20%.

*2.1.2.7. 4-(2-(4-(Trifluoromethyl)phenyl)pyrimidin-4-yl)morpholine (**5g**).* Off-white solid (57 mg, 83% yield). $R_f = 0.64$ (eluent = 100% EtOAc); FTIR ν_{max} / cm^{-1} (film) 3072, 2945, 1664, 1600, 1149, 1062; ^1H NMR (400 MHz, $CDCl_3$) δ_H: 8.49 (d, $J = 8.2$ Hz, 2H), 8.36 (d, $J = 6.2$ Hz, 1H), 7.70 (d, $J = 8.3$ Hz, 2H), 6.47 (d, $J = 6.2$ Hz, 1H), 3.88–3.78 (m, 4H), 3.78–3.67 (m, 4H); $^{13}C\{^1H\}$NMR (101 MHz, $CDCl_3$) δ_C: 162.1, 162.0, 155.6, 141.1, 132.2 (q, $J = 32.3$ Hz), 128.5, 125.4 (q, $J = 3.8$ Hz), 124.3 (q, $J = 272.3$ Hz), 101.6, 66.6, 44.3; $^{19}F\{^1H\}$NMR (376 Hz, $CDCl_3$) δ_F: $^-$62.7; Anal. calcd. for $C_{15}H_{14}F_3N_3O$ (309.11): C, 58.25; H, 4.56; N, 13.59%; found: C, 58.16; H, 4.60; N, 13.55%.

*2.1.2.8. 4-(2-(m-Tolyl)pyrimidin-4-yl)morpholine (**5h**).* Off-white solid (60 mg, 95% yield). $R_f = 0.54$ (eluent = 100% EtOAc); FTIR ν_{max} / cm^{-1} (film) 3069, 2971, 1672, 1605, 1154, 1039; ^1H NMR (400 MHz, $CDCl_3$) δ_H: 8.32 (d, $J = 6.2$ Hz, 1H), 8.17 (d, $J = 8.3$ Hz, 2H), 7.33 (t, $J = 7.5$ Hz, 1H), 7.28–7.22 (m, 1H), 6.39 (d, $J = 6.2$ Hz, 1H), 3.85–3.76 (m, 4H), 3.72–3.69 (m, 4H), 2.41 (s, 3H); $^{13}C\{^1H\}$NMR (101 MHz, $CDCl_3$) 162.0, 155.6, 138.1, 131.4, 128.7, 128.6, 128.5, 128.4, 125.4, 100.9, 66.6, 44.2, 21.6; Anal. calcd. for $C_{15}H_{17}N_3O$ (255.14): C, 70.56; H, 6.71; N, 16.46%; found: C, 70.48; H, 6.64; N, 16.37%.

*2.1.2.9. 4-(2-(2-Methoxyphenyl)pyrimidin-4-yl)morpholine (**5i**).* Light yellow viscous liquid (65 mg, 97% yield). $R_f = 0.19$ (eluent = 100% EtOAc); FTIR ν_{max} / cm^{-1} (film) 3057, 2979, 1660, 1623, 1169, 1029; ^1H NMR (400 MHz, $CDCl_3$) δ_H: 8.41 (d, $J = 6.3$ Hz, 1H), 7.71 (dd, $J = 7.6$, 1.7 Hz, 1H), 7.51 (td, $J = 7.3$, 1.3 Hz, 1H), 7.05–6.96 (m, 2H), 6.44 (d, $J = 6.3$ Hz, 1H), 3.87 (s, 3H), 3.79–3.72 (m, 4H), 3.70–3.63 (m, 4H); $^{13}C\{1H\}$NMR (101 MHz, $CDCl_3$) δ_C: 161.9, 157.9, 155.1, 132.2, 132.1, 128.6, 128.5, 120.5, 112.1, 100.4, 66.6, 56.2, 44.2; Anal. calcd. for $C_{15}H_{17}N_3O_2$ (271.13): C, 66.40; H, 6.32; N, 15.49%; found: C, 66.31; H, 6.21; N, 15.40%.

*2.1.2.10. 4-(2-(Naphthalen-1-yl)pyrimidin-4-yl)morpholine (**5j**).* Yellow viscous liquid (70 mg, 96% yield). $R_f = 0.46$ (eluent = 100% EtOAc); FTIR ν_{max} / cm^{-1} (film) 3061, 2998, 1648, 1602, 1176, 1037; ^1H NMR (400 MHz, $CDCl_3$) δ_H: 8.44 (d, $J = 6.2$ Hz, 1H), 8.03 (dd, $J = 7.2$, 1.0 Hz, 1H), 7.96–7.86 (m, 2H), 7.60–7.44 (m, 4H), 6.48 (d, $J = 6.3$ Hz, 1H), 3.82–3.75 (m, 4H), 3.75–3.64 (m, 4H); $^{13}C\{^1H\}$NMR (101 MHz, $CDCl_3$) δ_C: 165.9, 161.9, 155.6, 134.1, 132.1, 131.1, 130.2, 128.8, 128.5, 126.5, 126.1, 125.8, 125.2, 100.6, 66.6, 44.3; Anal. calcd. for $C_{18}H_{17}N_3O$ (291.14): C, 74.20; H, 5.88; N, 14.42%; found: C, 74.09; H, 5.81; N, 14.33%.

*2.1.2.11. (E)-4-(2-styrylpyrimidin-4-yl)morpholine (**5k**).* Off-white solid (40 mg, 60% yield). $R_f = 0.35$ (eluent = 100% EtOAc); FTIR ν_{max} / cm^{-1} (film) 3039, 2986, 1678, 1667, 1613, 1165, 1071; ^1H NMR (400 MHz, $CDCl_3$) δ_H: 8.23 (d, $J = 6.2$ Hz, 1H), 7.87 (d, $J = 16.0$ Hz, 1H), 7.59 (d, $J = 7.2$ Hz, 2H), 7.38–7.29 (m, 3H), 7.09 (d, $J = 16.0$ Hz, 1H), 6.34 (d, $J = 6.2$ Hz, 1H), 3.88–3.75 (m, 4H), 3.74–3.60 (m, 4H); $^{13}C\{^1H\}$NMR (101 MHz, $CDCl_3$) δ_C: 163.5, 161.8, 155.2, 137.6, 136.2, 129.0, 128.8, 127.7 (2 × C), 100.7, 66.6, 44.2; Anal. calcd. for $C_{16}H_{17}N_3O$ (267.14): C, 71.89; H, 6.41; N, 15.72%; found: C, 71.80; H, 6.34; N, 15.66%.

*2.1.2.12. 4-(2-Vinylpyrimidin-4-yl)morpholine (**5l**).* Light yellow viscous liquid (31 mg, 65% yield). $R_f = 0.32$ (eluent = 100% EtOAc); FTIR ν_{max} / cm^{-1} (film) 3067, 2951, 1657, 1604, 1180, 1042; ^1H NMR (400 MHz, $CDCl_3$) δ_H: 8.23 (d, $J = 6.2$ Hz, 1H), 6.69 (dd, $J = 17.3$, 10.4 Hz, 1H), 6.48 (dd, $J = 17.3$, 2.0 Hz, 1H), 6.34 (d, $J = 6.2$ Hz, 1H), 5.60 (dd, $J = 10.4$, 2.0 Hz, 1H), 3.81–3.76 (m, 4H), 3.67–3.57 (m, 4H); $^{13}C\{^1H\}$NMR (101 MHz, $CDCl_3$) δ_C: 163.6, 161.9, 156.1, 137.4, 122.7, 101.2, 66.7, 44.1; Anal. calcd. for $C_{10}H_{13}N_3O$ (191.11): C, 62.81; H, 6.85; N, 21.97%; found: C, 62.71; H, 6.79; N, 21.90%.

2.2. X-ray characterization

Compound **5e** was characterized through X-ray crystallography. The full refinement parameters and crystal data (Table S3) are given in Supplementary material.

2.3. In vitro cholinesterase inhibition assay

Spectrophotometric methods reported by Ellman [58] with slight alterations were used to measure the *in vitro* inhibitory potential of AChE and BuChE enzymes. A solution of 60 μL of phosphate buffer (KH_2PO_4/KOH, pH = 7.7), 10 μL of test compound dissolved in DMSO (2%) and 10 μL of enzymes (0.5 and 3.4 U/mg of AChE or BuChE) were included in the reaction mixture. Pre-incubation was carried out at 37 °C for 10 min with the reaction contents thoroughly mixed. Following the pre-incubation, the reaction was initiated by the addition of 1 mM acetylthiocholine chloride or butyrylthiocholine chloride to the enzymatic solution of AChE or BuChE, respectively. Further incubation at 37 °C for 20 min was conducted on the mixture with DTNB (10 mL, 0.5 mM). The absorbance was recorded at 405 nm with a 96-well microplate reader. Each reaction was performed in triplicate. Assay was conducted using a blank in the absence of inhibitor to measure enzymatic activity. Inhibition percentage was determined using the formula given below:

$$\%\text{Inhibition} = 100 - (\text{absorbance of compound/absorbance of standard}) \times 100$$

The IC_{50} values were calculated using PRISM 5.0 based on non-linear curve fitting of compounds with > 50% inhibition against acetylcholinesterase and butyrylcholinesterase (GraphPad, San Diego, California, USA).

2.4. Kinetics protocol

We determined the type of inhibition of AChE enzyme by using Michaelis-Menten kinetics. For the investigation of the potential mechanism of action of compound **5h**, detailed kinetics study was performed. In order to determine the inhibition rate of enzyme at four different concentrations of substrate (0.25, 0.5, 1.0, 1.5 mM) and compound **5h**

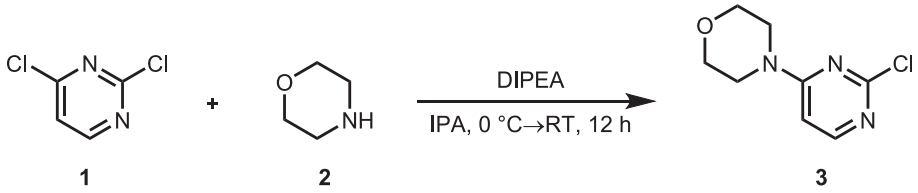

Scheme 1. Synthesis of 4-(2-chloropyrimidin-4-yl)morpholine **3**.

(0, 0.2, 0.4, 0.6 μM), the initial inhibition rates were measured against acetylcholinesterase.

2.5. In silico modeling protocols

2.5.1. Selection and preparation of compounds

In order to analyze the potential interactions between the inhibitors and cholinesterase enzymes, molecular docking analysis was performed. Using the RCSB PDB database, the structure of hAChE (PDBID:4BDT) and hBuChE (PDBID:4BDS) was retrieved for docking studies [59,60]. In order to simulate the enzyme and compounds, the structure of the AChE was protonated using the Protonate3D [61] algorithm executed within the MOE [62]. All crystallographic solvent molecules were taken into account in the Amber99 force field when minimizing the energy of the structure. A small force was applied to the backbone atoms during energy minimization calculations to avoid the active site from collapsing. Subsequently, ligands and solvent molecules were removed. By using MOE, the X-ray structure has been modified to include hypothetical hydrogen atoms in standard geometries in place of the crystallographic water molecules.

2.5.2. Preparation of compounds

In the "wash" module, 3D structural coordinates have been generated for compounds based on the MOE method, and the protonation and ionization states have been assigned to those compounds in the physiological pH range. Consequently, MMFF94x force fields were applied to minimize energy of structures for molecular docking analysis.

2.5.3. Docking analysis

In silico docking analysis was carried out by using LeadIT, a software program from BioSolveIT Germany, GmbH [63]. Load or Prepare Receptor utility of LeadIT suite was used to load the receptor. As a result of the spacing of amino acids in 9.0 Å, the binding pocket for the receptor is defined. Pyrimidine-morpholine hybrids were docked using the software FlexX utility of LeadIT. Using binding free energies, 50 conformations of ligand-receptor complexes were produced for each compound docked within the receptor binding site. A maximum of top 30 docked poses were kept for further analysis based on default docking parameters [64]. We considered poses depicting the least free energies to be the most stable, demonstrating the strongest receptor interactions. Discovery Studio Visualizer v4 was used to visualize 3D putative interactive modes of protein–ligand complexes with least binding energies [65].

2.6. Molecular dynamics simulation protocol

The crystallographic structures for hAChE (PDB ID: 4BDT) and hBuChE (PDB ID: 4BDS) were retrieved from the Protein Data Bank (https://www.pdb.org). In both protein structures, hydrogen atoms were added using an online webserver H++ [66] at pH 7.4. AMBER 20 utility of tleap [67] was used to generate force field parameters for protein structure using the ff14SB force field [68]. Antechamber and parmchk2 modules of the AMBER software package were used to generate the second generation Generalized AMBER force field (GAFF2) with AM1-BCC charge [69,70]. In the following step, both protein structures (4BDT and 4BDS) in Apo form and **5h** bound form were dissolved in 70 Å TIP3P [71] water molecules and neutralized with Na^+ and Cl^{-1} ions whose parameters were calculated based on literature [72]. The final step was to generate the coordinates and parameters for these four systems in AMBER software using xleap module.

AMBER 20 is used to run all MD simulations utilizing the Particle Mesh Ewald Molecular Dynamics module (PMEMD) [67]. Based on a 2.0 kcal mol^{-1} cut-off, 2000 steps of steepest decent minimization were used to minimize the system. To equilibrate these systems, a 1 ns NPT simulation using the Berendsen barostate and removed backbone potential restraints was performed after 400 ps of heating the system from 0 to 298.15 K using the Langevin thermostate [73,74]. In the next step, a 50 ns NPT MD simulation was performed with 2 fs time steps employing the SHAKE protocol on hydrogen atoms as well as a 10 Å non-bonded cut-off with periodic boundary conditions/parameters. Pytraj and Cpptraj of the AMBER module [75], and the VMD software [76], respectively, were used to analyze and visualize the data at each 2.5 ps.

3. Results and discussion

3.1. Preparation of 4-(2-chloropyrimidin-4-yl)morpholine (3)

2,4-Dichloropyrimidine, morpholine and DIPEA were stirred in IPA at room temperature to afford compound **3** in 82% isolated yield (Scheme 1). The spectroscopic data fully supported the formation of compound **3** and was in accordance with that stated in the literature [57]. Compound **3** was used as the main starting material for coupling with a diverse range of boronic acids/esters to produce the target compounds.

3.2. Palladium-catalyzed Suzuki coupling

The formation of target compounds (**5a-l**) was achieved by arylation of compound **3** with a variety of boronic acids under Suzuki-Miyaura cross coupling conditions. 1,1′-Bis(diphenylphosphino)ferrocenedichloropalladium(II) was used as a promising catalyst. The reaction conditions illustrated in Table 1 successfully delivered a range of desired products in 55–97% isolated yields. The reaction scope includes various aromatic and alkenylated boronic acid nucleophiles (**4a-l**) in combination with 1–4-(4-chloropyrimidin-2-yl)morpholine (**3**) as the coupling partner. Aryl boronic acids incorporating electron-donating (OMe, Me) and electron-withdrawing (F, Cl, CF_3, Ac) functional groups were successful coupling partners and delivered the corresponding biaryl products in good to excellent yields. The molecular structure of compound **5e** was explicitly established by single crystal X-ray crystallography (Fig. 2). Various substituents at *para*-, *meta*- and *ortho*-position of phenyl ring were well tolerated. The use of *tert*-butyl-substituted phenylboronic acid smoothly provided the biaryl core, albeit in moderate yield (55%). A bulky naphthyl boronic acid also underwent carbon–carbon bond formation and yielded the corresponding product in 95% isolated yield. Styrylboronic acid as well as vinylboronic acid pinacol ester were also envisioned as suitable coupling partners and furnished the desired products in 60% and 65% yield, respectively. Overall, this protocol provides promising small molecules for further applications in drug discovery.

Table 1
Scope of palladium-catalyzed Suzuki-Miyaura cross-coupling reaction.[a,b]

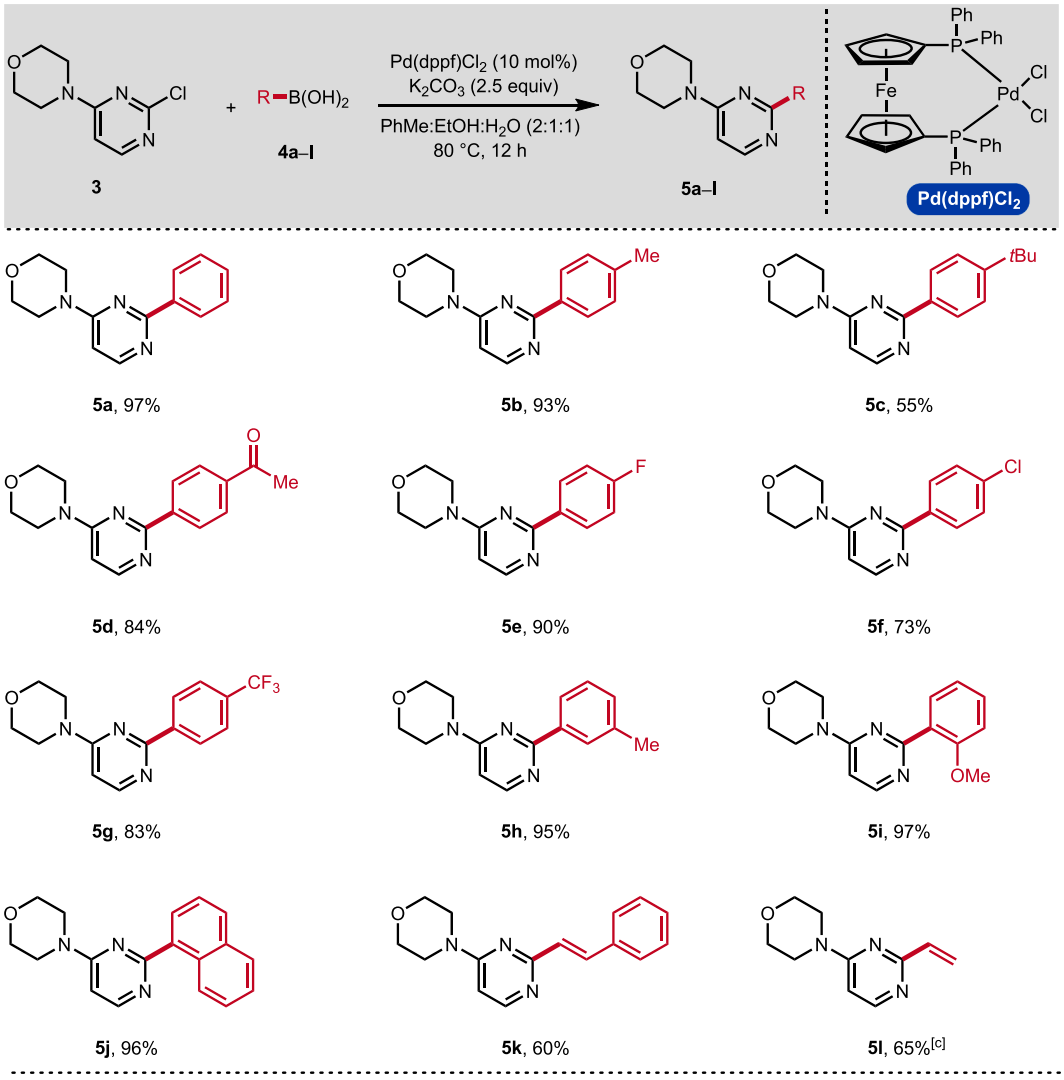

[a]Reactions performed using 0.25 mmol of 4-(2-chloropyrimidin-4-yl)morpholine starting material. [b]Isolated yields. [c]Vinylboronic acid pinacol ester was used.

3.3. Anti-cholinesterase profile and structure-activity relationships

The newly synthesized pyrimidine-morpholine hybrids (**5a-l**) were subjected to *in vitro* biochemical assays to evaluate their inhibitory potential against acetylcholinesterase and butyrylcholinesterase enzymes using Ellman's protocol [58]. Neostigmine and donepezil were chosen as standard drugs for comparison purposes. *In vitro* cholinesterase inhibitory data for the synthetic compounds are shown in Table 2. The synthesized compounds consist of three components: 1) heterocyclic pyrimidine as the central scaffold; 2) morpholine ring attached at the 4-position of pyrimidine heterocycle; and 3) variable (R) group at 2-position of pyrimidine core for the introduction of structural variations. In particular, the pyrimidine ring remains crucial in establishing vital interactions like conventional hydrogen bonding. Morpholine oxygen atom also establishes hydrogen bond whereas the introduction of an aromatic substituent (R) at 2-position of pyrimidine heterocycle as well as pyrimidine ring itself found to be involved in π-π stacking. So, the biologically potent synthesized compounds and their structural variations are vital for the establishment of several important contacts with various active site bound amino acids of both enzymes (AChE and BuChE). As the cholinesterase inhibition profile (*in vitro*) represented herein reveals a distinct picture, the exploration of SAR analyses against cholinesterases are of paramount importance in guiding the drug discovery efforts to the next level. The inhibitory activity data displayed in Table 2 also demonstrates the vital significance of the substituent (R) for strong potency.

All the tested compounds showed potent inhibitory potential towards acetylcholinesterase within the range of 0.43–8.66 μM. The existence of a *meta*-tolyl substituent at 2-position of pyrimidine ring (**5h**) was remarkably preferred over other substituents and identified as the principal candidate with the best efficacy having an IC_{50} value of 0.43 ± 0.42 μM, which is ~ 38-fold stronger inhibitory potency as compared to the standard drug (neostigmine; IC_{50} = 16.2 ± 1.01 μM). The effect of switching position of methyl substituent from *meta*- to *para*-position in compound **5b** was detrimental, however, the acquired efficacy was still ~ 3-fold higher than neostigmine. On the contrary, the replacement of methyl group with a *tert*-butyl substituent improved the inhibition profile (**5c**; IC_{50} = 3.4 ± 0.21 μM). Next, the introduction of electron-withdrawing groups such as acetyl showed effective inhibitory strength with an inhibition value of 1.4 ± 0.11 μM, ~12-fold robust

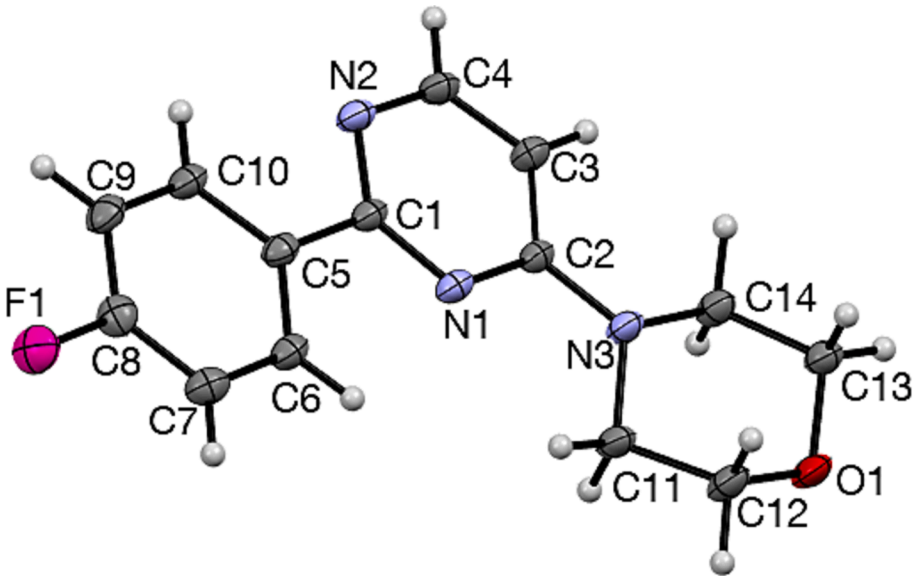

Fig. 2. ORTEP structure of compound **5e** (CCDC 2261470).

Table 2
Evaluation of AChE and BuChE inhibitory potential of pyrimidine-morpholine hybrids **5a-l**.

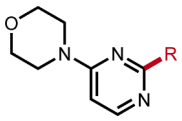

Compound	R group	AChE inhibition	BuChE inhibition
		IC_{50} ± SEM (μM)/%inhibition	
5a	Ph	8.66 ± 0.52	32
5b	4-Me-Ph	5.6 ± 0.42	37
5c	4-*t*Bu-Ph	3.4 ± 0.21	40
5d	4-Ac-Ph	1.4 ± 0.11	17
5e	4-F-Ph	0.78 ± 0.11	23
5f	4-Cl-Ph	2.8 ± 0.12	43
5g	4-CF_3-Ph	3.9 ± 0.22	27
5h	3-Me-Ph	0.43 ± 0.02	2.5 ± 0.12
5i	2-OMe-Ph	6.2 ± 0.50	8.9 ± 0.62
5j	1-Np	6.1 ± 0.47	28.7 ± 2.23
5k	styryl	2.9 ± 0.22	13.4 ± 0.22
5l	vinyl	5.0 ± 0.40	34
Neostigmine	–	16.2 ± 1.01	–
Donepezil	–	–	7.19 ± 0.14

inhibition efficacy than standard drug whereas trifluoromethyl substituent was little less effective (IC_{50} = 3.9 ± 0.22 μM). Replacing the acetyl with fluoro substituent further improved the inhibitory potency rendering compound **5e** as the selective AChE inhibitor and the second most potent lead among the tested derivatives with an IC_{50} value of 0.78 ± 0.11 μM. A halogen swap with chloro substituent led to a drop in potency but still better than neostigmine. Introduction of an *ortho*-methoxyphenyl (**5i**) and 1-naphthyl (**5j**) rings produced similar results with inhibitory values of 6.2 ± 0.50 and 6.1 ± 0.47 μM, respectively. Compound **5k** bearing a styryl group exhibited a potent anti-cholinesterase efficacy depicting an inhibitory value of 2.9 ± 0.22 μM. The removal of a phenyl ring at alkene moiety generating a vinyl moiety demonstrated a slight reduction in activity but still better than several inhibitors. Finally, the least inhibition was demonstrated by compound **5a** bearing an unsubstituted phenyl ring at 4-position of pyrimidine scaffold.

In parallel, the synthesized pyrimidine-morpholine hybrid derivatives (**5a-l**) were also evaluated against butyrylcholinesterase enzyme to determine their inhibitory potential. Against BuChE, only few derivatives depicted good inhibition indicating **5h** as the top candidate with an inhibition potency of 2.5 ± 0.04 μM, ~3-fold stronger result than positive control, donepezil (IC_{50} = 7.19 ± 0.14 μM). This compound possessed a *meta*-tolyl as a substituent at 2-position of pyrimidine ring which fits enough in the active binding site of butyrylcholinesterase. Another active compound against butyrylcholinesterase enzyme was **5i** bearing an *ortho*-methoxyphenyl ring which revealed a comparable inhibitory potential with an IC_{50} value of 8.9 ± 0.05 μM compared to donepezil. Compound **5e** bearing a 1-naphthyl ring illustrated detrimental inhibition (IC_{50} = 28.7 ± 0.05 μM) whereas compound **5j** (IC_{50} = 13.4 ± 0.02 μM) with a styryl substituent showed reduced efficacy against butyrylcholinesterase compared to donepezil. The remaining derivatives in the series showed < 50% inhibition against butyrylcholinesterase in the range of 17–43%.

3.4. Mechanism of inhibition

Kinetics studies were performed to determine the mode of action of compound **5h** against acetylcholinesterase. Acetylthiocholine iodide was used as a substrate. To determine the type of inhibition, analyze the effect of inhibitor on V_{max} and K_m, a Lineweaver-Burk plot (reciprocal of reaction rates 1/V and reciprocal of substrate concentrations 1/S) was used.

Different concentrations of inhibitor **5h** and substrate were used to perform kinetics analysis. Four concentrations (0, 0.2, 0.4, 0.6 μM) of inhibitor **5h** and four concentrations (0.25, 0.5, 1.0, 1.5 mM) of substrate were used. Compound **5h** exhibited the non-competitive inhibition with acetylthiocholine iodide within the active pocket of AChE. V_{max} of the enzyme was decreased and K_m of the substrate was not affected which depicted a non-competitive inhibition as shown in Fig. 3. In the non-competitive inhibition, the inhibitor molecule binds to a site on the enzyme other than the active site, which affects the overall structure of the enzyme and reduces its activity. The binding of the inhibitor does not directly compete with the substrate for binding to the active site, so increasing the substrate concentration will not affect the inhibition.

3.5. Molecular docking analysis

The docking studies were carried out for the potent compounds (**5d**, **5e** and **5h**) within the active site of acetylcholinesterase and butyrylcholinesterase to analyze important interactions with the protein 4BDT [59] and 4BDS [60]. Compounds **5d** and **5e** were selective inhibitors of acetylcholinesterase whereas **5h** was a dual inhibitor of both cholinesterases (AChE and BuChE). The docking studies of potent inhibitor **5d** within active binding site of acetylcholinesterase represented different vital interactions with amino acid residues like TRP439, TYR124, ASP74, TRP86 and TYR337. The docking of compound **5d** within the catalytic region of acetylcholinesterase revealed the formation of conventional hydrogen bond between ASP74 and oxygen atom of morpholine ring with a distance of 3.05 Å. Carbon hydrogen bond and π-alkyl interaction were also noticed between morpholine ring and TYR124 docked competitively within the active pocket having a distance of 3.51 and 5.45 Å, respectively. TRP86 also established a C—H bond with the morpholine moiety with a distance of 3.09 Å as well as two π-π stacked interactions with pyrimidine ring (4.69 Å) and acetophenone (4.30 Å) moiety. π-Sigma bond was also observed with TRP439 showing a distance of 3.81 Å. Finally, TYR337 was involved in the formation of a π-π stacked interaction with the acetophenone moiety with a distance of 3.72 Å as presented in Fig. 4.

Another potent inhibitor **5e** was also docked within the active binding site of acetylcholinesterase and exhibited various crucial interactions with amino acid residues such as SER125, ASP74, TYR337, TYR133 and TRP86. Morpholine moiety depicted multiple interactions within the active pocket of acetylcholinesterase involving SER125 (3.22 Å) and TYR133 (3.53 Å) by forming the carbon hydrogen bonds while TRP86 (4.47 Å) exhibited π-alkyl interaction. On the other hand, pyrimidine ring was arranged against TRP86 through π-π stacked interaction (4.31 Å), ASP74 showed a carbon hydrogen bond (3.53 Å), while, TYR337 depicted conventional hydrogen bond (3.07 Å) and a π-donor hydrogen bond (3.66 Å). Furthermore, fluorobenzene ring also revealed a π-π stacked interaction with the amino acid residues such as TRP86 and TYR337 with the distance of 4.80 and 3.63 Å, respectively, as shown in Fig. 5.

Finally, the docking of most potent inhibitor **5h** within the binding site of acetylcholinesterase depicted different vital interactions with the amino acid residues such as TRP86, TYR337, TRP439, TYR449 and PRO446. Upon analysis of docking results of compound **5h**, it was noted that TRP86 was involved in the formation of multiple interactions such as π-π stacking, C—H bond and π-alkyl bond with the active moieties of the compound. TRP86 exhibited π-π stacked interactions with pyrimidine ring (4.03 Å) and *m*-tolyl moiety (4.64 Å) as well as π-alkyl (4.52 Å) and C—H bond (3.44 Å) interactions. Similarly, TYR337 also depicted a π-π stacked interaction (3.63 and 5.63 Å) with the *m*-tolyl moiety and pyrimidine ring of **5h**, respectively. Moreover, alkyl linkages were also established with amino acid residues including TYR337 (4.35 Å), TRP439 (4.80 Å), TYR449 (4.76 Å) and PRO446 (4.29 Å) as shown in Fig. 6.

Similarly, the docking study of the lead BuChE inhibitor **5h** inside the active pocket of butyrylcholinesterase also revealed multiple interactions such as π-π *T*-shaped, amide-π stacked, alkyl linkage, π-alkyl, conventional hydrogen bond and carbon hydrogen bond. The active moiety of compound **5h**, *m*-tolyl, exhibited π-π *T*-shaped interactions

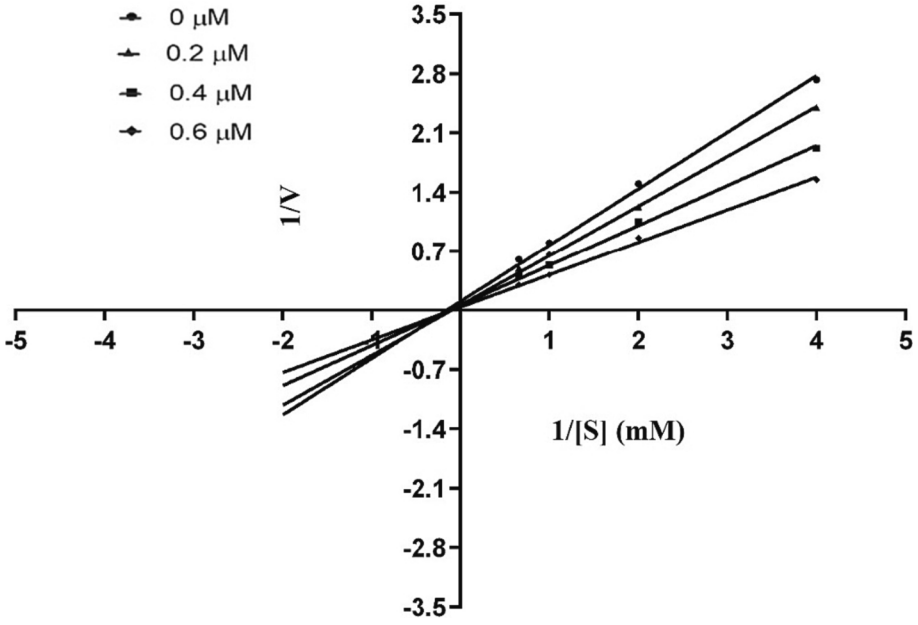

Fig. 3. Inhibition mode of compound **5h** against AChE.

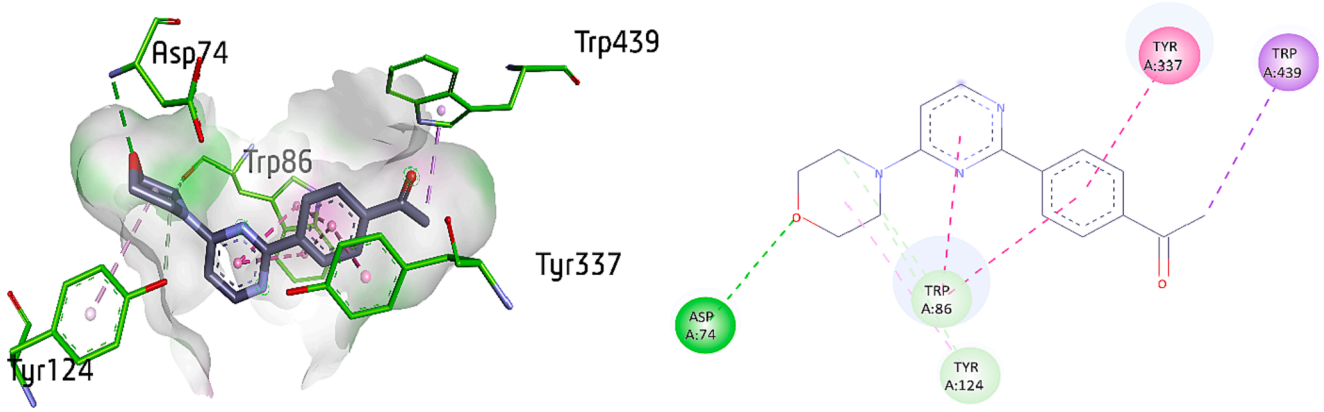

Fig. 4. 2D and 3D interaction poses of docked compound **5d** against AChE; hydrogen bond as green, π-alkyl as light pink, π-π stacking interactions are shown as fuchsia, carbon hydrogen bond as light green and π-sigma as purple dotted lines. (For interpretation of the references to color in this figure legend, the reader is referred to the web version of this article.)

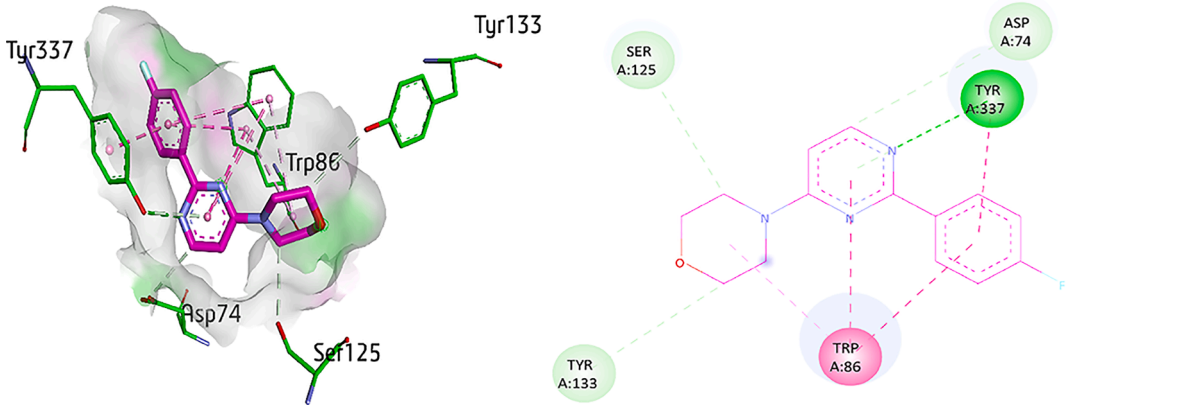

Fig. 5. 2D and 3D interaction poses of docked compound **5e** against AChE; hydrogen bond as green, π-alkyl as light pink, π-π stacking interactions are shown as fuchsia, carbon hydrogen bond as light green and π-sigma as purple dotted lines. (For interpretation of the references to color in this figure legend, the reader is referred to the web version of this article.)

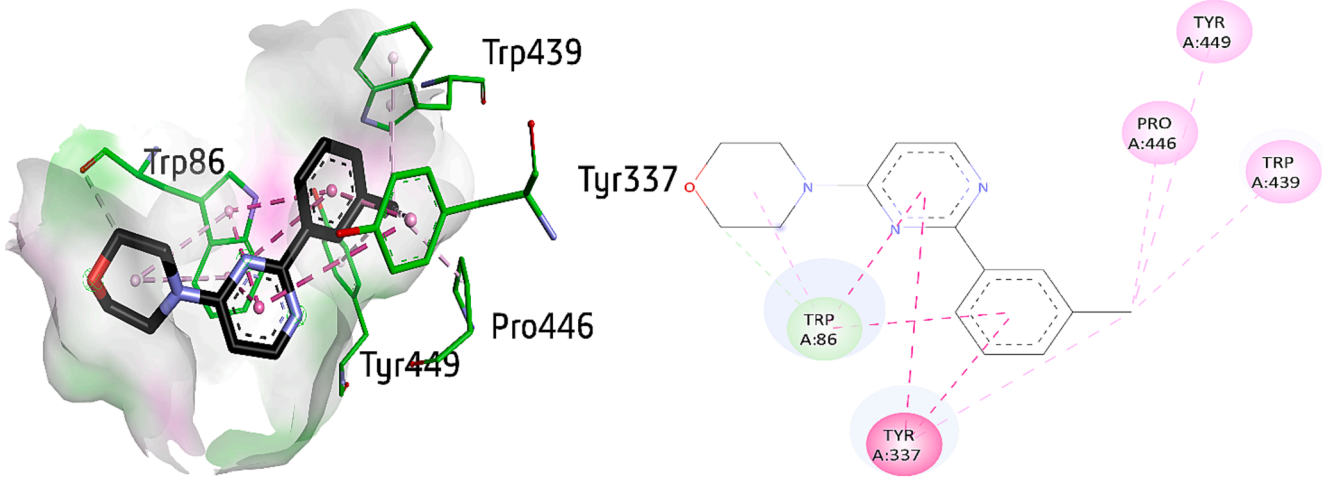

Fig. 6. 2D and 3D interaction poses of docked compound **5h** against AChE; hydrogen bond as green, π-alkyl as light pink, π-π stacking interactions are shown as fuchsia, carbon hydrogen bond as light green and π-sigma as purple dotted lines. (For interpretation of the references to color in this figure legend, the reader is referred to the web version of this article.)

with TRP231 (6.72 Å) and PHE329 (5.11 Å), amide-π stacked with GLY116 (5.09 Å), alkyl interaction with VAL288 (5.09 Å) and a π-alkyl interaction with LEU286 with a distance of 5.28 Å. Furthermore, pyrimidine ring also depicted π-π *T*-shaped interactions with HIS438 and conventional hydrogen bond with SER198 having a distance of 4.37 and 3.08 Å, respectively, whereas, morpholine ring offered multiple bonding

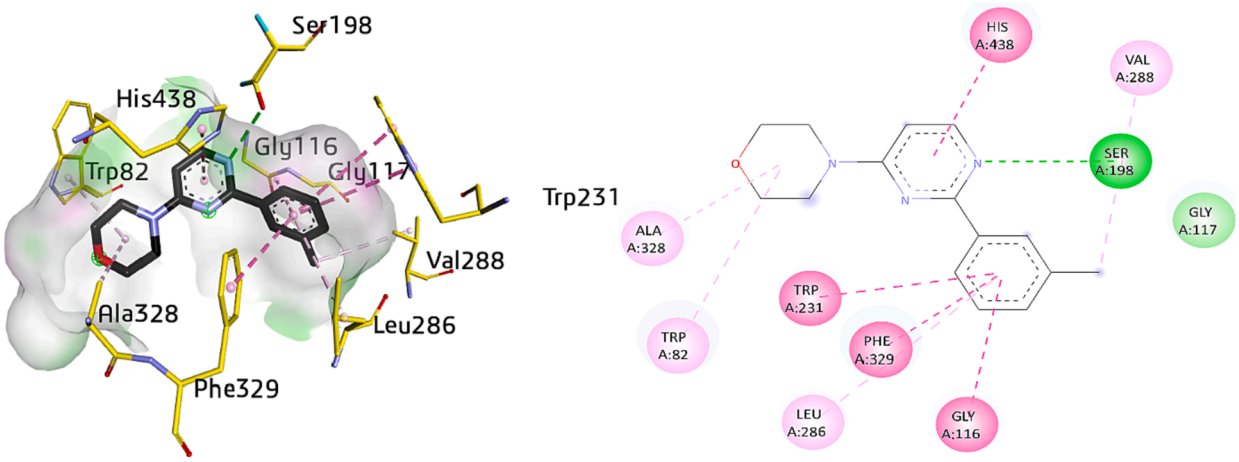

Fig. 7. 2D and 3D interaction poses of docked compound **5h** against BuChE; hydrogen bond as green, π-alkyl as light pink, π-π stacking interactions are shown as fuchsia, carbon hydrogen bond as light green and π-sigma as purple dotted lines. (For interpretation of the references to color in this figure legend, the reader is referred to the web version of this article.)

such as π-alkyl linkages with the amino acid residues such as TRP82 (4.93 Å) and ALA328 (4.36 Å) as shown in Fig. 7.

The distance of bonds, binding interactions types and atoms playing role in interactions for AChE and BuChE are illustrated in Table 3.

Table 3
Distance of bonds, types of binding interactions and atoms playing role in interactions (AChE and BuChE).

Compounds	Binding interactions			
	Ligand atom	Receptor residue	Interaction type	Distance (Å)
5d (AChE)	O3	ASP74	H-bond	3.05
	C21	TRP439	π-sigma	3.81
	Morpholine	TRP86	C—H bond	3.09
	Morpholine	TYR124	C—H bond	3.51
	Morpholine	TYR124	π-alkyl	5.45
	Pyrimidine	TRP86	π-π stacked	4.69
	Phenyl	TRP86	π-π stacked	4.30
	Phenyl	TYR337	π-π stacked	3.72
5e (AChE)	N13	TYR337	H-bond	3.07
	Morpholine	SER125	C—H bond	3.22
	Morpholine	TYR133	C—H bond	3.53
	Morpholine	TRP86	π-alkyl	4.47
	Phenyl	TYR337	π-π stacked	3.63
	Phenyl	TRP86	π-π stacked	4.80
	Pyrimidine	ASP74	C—H bond	3.53
	Pyrimidine	TRP86	π-π stacked	4.31
	Pyrimidine	TYR337	π-donor H-bond	3.66
5h (AChE)	C4	TRP86	C—H bond	3.44
	C19	PRO446	Alkyl	4.29
	C19	TYR337	Alkyl	4.35
	C19	TRP439	Alkyl	4.80
	C19	TYR449	Alkyl	4.76
	Morpholine	TRP86	π-alkyl	4.52
	Pyrimidine	TRP86	π-π stacked	4.03
	Pyrimidine	TYR337	π-π stacked	5.63
	Phenyl	TRP86	π-π stacked	4.64
	Phenyl	TYR337	π-π stacked	3.63
5h (BuChE)	N13	SER198	H-bond	3.08
	C19	VAL288	Alkyl	5.09
	Phenyl	GLY116	amide-π stacked	5.09
	Phenyl	PHE329	π-π *T*-shaped	5.11
	Phenyl	TRP231	π-π *T*-shaped	6.72
	Phenyl	LEU286	π-alkyl	5.28
	Pyrimidine	HIS438	π-π *T*-shaped	4.37
	Morpholine	ALA328	π-alkyl	4.36
	Morpholine	TRP82	π-alkyl	4.93

3.6. SeeSAR visual drug design

SeeSAR visual investigation was carried out for all synthesized compounds, however, only **5e** and **5h** exhibited remarkable Hyde energies against acetylcholinesterase. The visual and deeply docked poses of inhibitors **5e** and **5h** depicted expressible, innovative and significant conformations employing SeeSAR [64]. Fig. 8 depicts the interactive and refractive optimization of hits revealing the non-binding and binding capability of inhibitors. Various atoms such as carbon, oxygen and nitrogen exhibited Hyde energies in compounds **5e** and **5h**. Desolvation and interactions for potent compounds **5e** (C5: −2.5 kj/mol, C14: −2.4 kj/mol, C17: −4.1 kj/mol F19: −5.9 kj/mol and C18: −2.7 kj/mol) and **5h** (*C2*: −3.0 kj/mol, C10: −1.8 kj/mol, C14: −2.3 kj/mol, C16: −5.0 kj/mol, C18: −2.1 kj/mol and C19: −8.5 kj/mol) were also observed. The approach reveals the visual and illustratable assessment for implied H-bonds and dehydration achieved through FlexX default parameters, and validates the results of docking studies.

3.7. Molecular dynamics simulations

Additionally, molecular dynamics simulations were performed for the most potent compound **5h** against cholinesterases (AChE and BuChE), which demonstrates several fold higher inhibitory potential than the remaining compounds. The molecular dynamics simulation of protein complexes with the potent compound **5h** was performed in aqueous medium for 50 ns under the initial conformations taken from the best docked pose which exhibited lowest binding energy as well as the best binding affinity in active pocket of AChE and BuChE were observed within specific time dependent mode.

The stability of receptor and its relationship with inhibitor are represented by RMSD values as a result of MD simulations. Fig. 9a shows that potent compound **5h** (AChE) revealed more stability with little deviation in the range of 0–2.9 Å. Apo protein (4BDT) showed stability with a little deviation between 30 and 32 ns, however, the protein complex (4BDT + **5h**) exhibited good stability with the little deviations within the range of 8–9, 19–21, and 37–39 ns. The overall simulations were observed stable in comparison to apo protein (4BDT). It was noted that protein showed consistent fluctuation throughout the simulation. In parallel, compound **5h** (BuChE) revealed stability and slight deviation within the range of 0–1.8 Å. Apo protein (4BDS) showed stability with a little deviation between 0 and 6 ns whereas the structure of protein complex (4BDS + **5h**) exhibited overall stability with very little deviations within the range of 13–15 and 20–30 ns. The remaining simulations were observed stable as compared to apo protein (4BDS) as

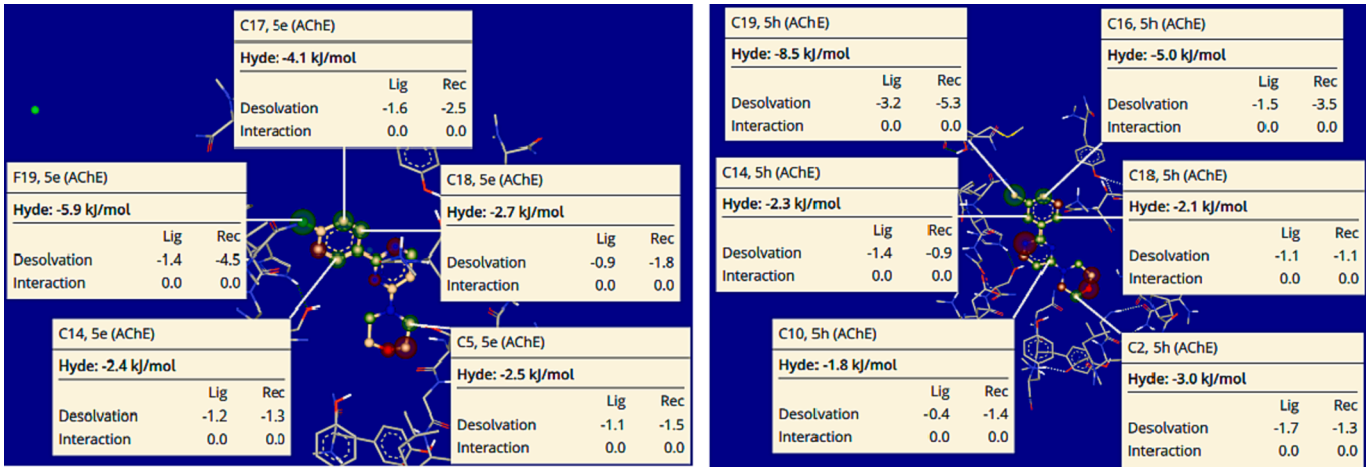

Fig. 8. Visualization and investigational modes of compounds **5e** (left) and **5h** (right) inside the active pocket of AChE (4BDT). The light green are chlorine atoms and blue are nitrogen atoms, however green color shows the favorable interactions and atoms contributing towards potency inside active site and oxygen atoms are shown in red. (For interpretation of the references to color in this figure legend, the reader is referred to the web version of this article.)

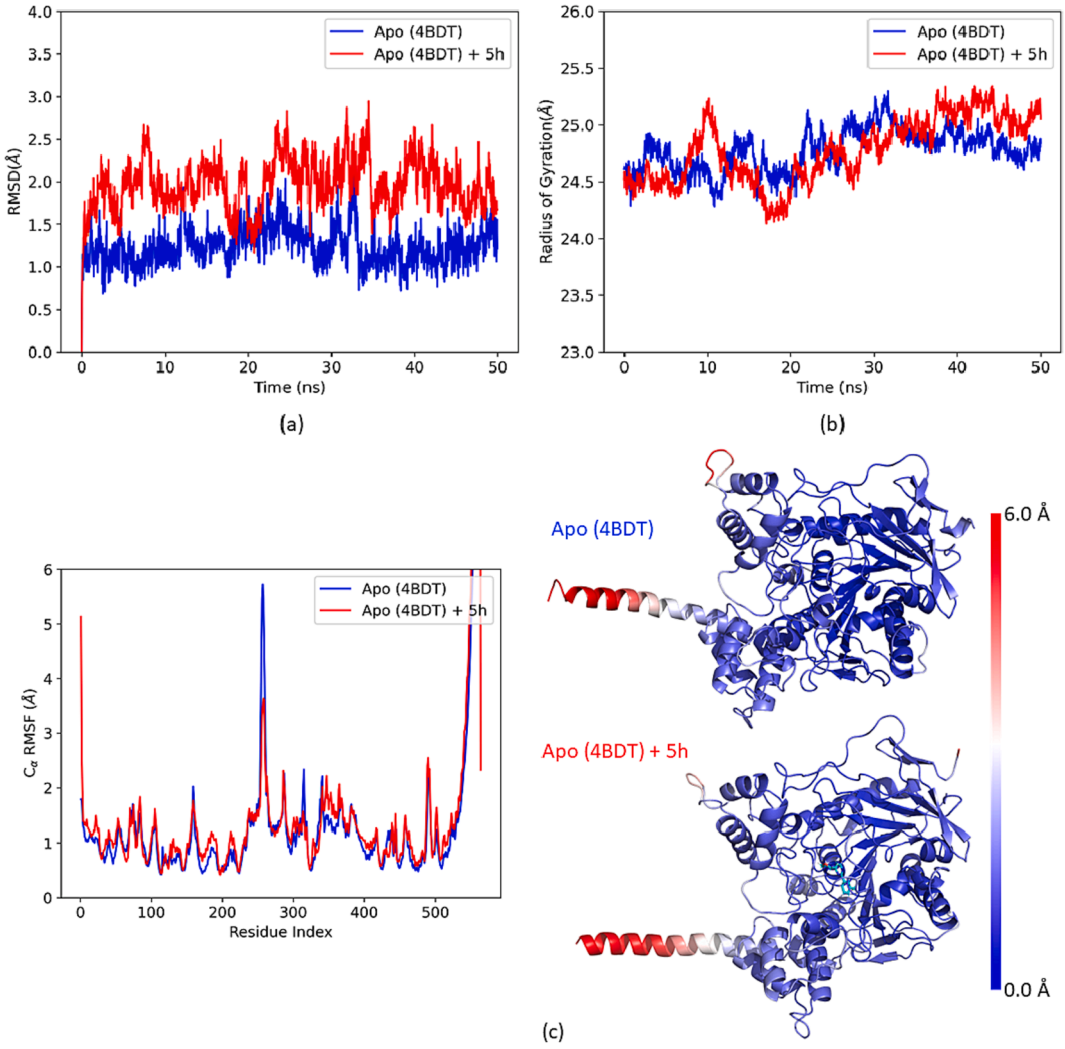

Fig. 9. Root mean square deviation (**a**), radius of gyration (**b**) root mean square fluctuation (**c**) of residues of receptor acetylcholinesterase (4BDT) in the time of 50 ns as time of simulation for compound **5h**.

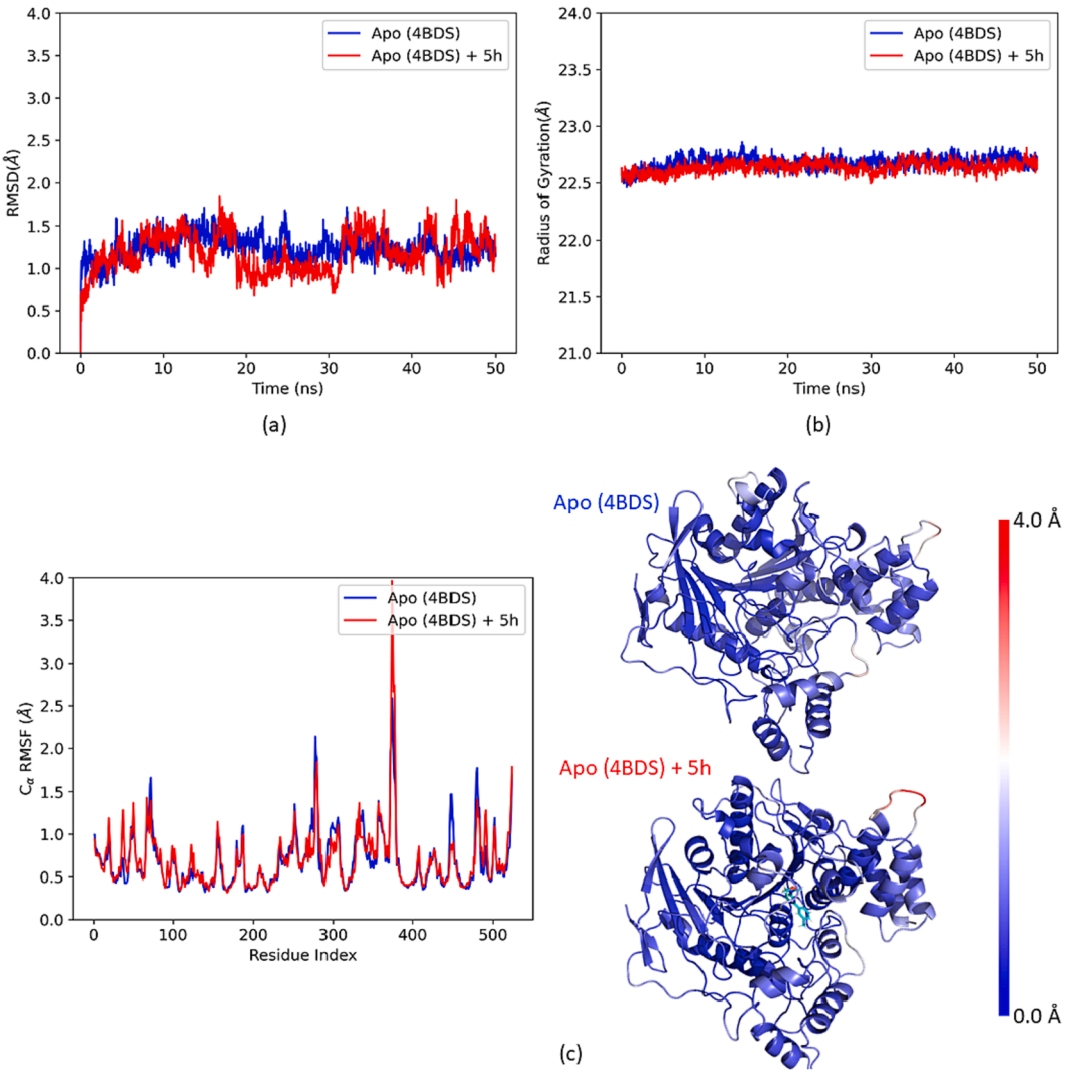

Fig. 10. Root mean square deviation (**a**), radius of gyration (**b**) root mean square fluctuation (**c**) of residues of receptor butyrylcholinesterase (4BDS) in the time of 50 ns as time of simulation for compound **5h**.

shown in Fig. 10a. Over the entire simulation period, protein showed consistent slight fluctuations.

MD simulation time was used to investigate the compactness of system based on its radius of gyration. Additionally, it describes how protein structures fold and unfold in the absence and presence of compound. The results in Fig. 9b revealed the protein compactness and presence of potent derivative. The average score of radii of gyration (Rg) for AChE and its complex with compound (4BDT + **5h**) was noted to 24.6 and 24.5 Å, respectively, and exhibited the compactness of structure in the whole simulation time. While, radii of gyration for BuChE and its complex (4BDS + **5h**) was noticed with almost the same score (22.6 Å) as shown in Fig. 10b.

By understanding root mean square fluctuations, we can determine how the protein structure will behave in the absence and presence of compound. As Fig. 9c depicted, apo protein and holo-protein showed the specific mode of fluctuation. The apo protein (4BDT) started from 1.0 Å and exhibited the fluctuation between 1.9 and 5.7 Å during the simulation time with slight increase to 6.0 Å, whereas, the holo-protein (4BDT + **5h**) started from 5.1 Å with fluctuation between 1.0 and 3.7 Å during the overall time of simulation with modest increase to 6.0 Å (Fig. 9c). In parallel, the apo protein (4BDS) began from 1.0 Å and exhibited the fluctuation around 1.0–2.2 Å during the time of simulation with small increase to 2.6 Å. Consequently, the holo protein (4BDS + **5h**) began from 0.9 Å and revealed the fluctuation around 0.9–1.9 Å during time of simulation with modest increase to 3.9 Å (Fig. 10c). Overall, the system displayed stability with fewer fluctuations. Over the simulation course, the region with loops and motifs displayed small fluctuation while the active pocket experienced significant stability. As compared to protein only, complex exhibited better stability.

3.8. *Physicochemical properties*

Pharmacokinetic properties of the potent inhibitors (**5d**, **5e** and **5h**) against AChE and BuChE were explored to evaluate effect of several parameters employing previously designed prediction software [77–80]. These parameters consist of polar surface area, molecular weight, number of acceptor atoms, number of donor atoms, lipophilicity, refractivity, partition coefficient such as *n*-octanol, log Po/w, WLOGP, MLOGP, and XLOGP etc. exploring the binding energies of solvation and solvent polar surface area [81]. One of most crucial parameters like molecular weight, was found to be < 500 Da, whereas hydrophobicity of the tested inhibitors such as polar surface area and Log P values representing the permeability of blood brain barrier. In parallel, hydrophilicity such as Log S value indicates the solubility of the compounds in aqueous environment. On the other hand, pharmacokinetics also exhibited gastrointestinal absorption, cytochrome inhibitors, P-gp

Table 4
ADMET prediction scores for the potent compounds (**5d**, **5e**, **5h**).

Properties	5d	5e	5h
Physicochemical properties			
Formula	$C_{16}H_{17}N_3O_2$	$C_{14}H_{14}FN_3O$	$C_{15}H_{17}N_3O$
Molecular weight	283.33	259.28	255.31
No. of heavy atoms	21	19	19
No. of aromatic heavy atoms	12	12	12
Fraction C(sp^3)	0.31	0.29	0.33
No. of rotatable bonds	3	2	2
No. of H-bond acceptors	4	4	3
No. of H-bond donors	0	0	0
Molar refractivity	83.39	73.15	78.16
TPSA (Å)	55.32	38.25	38.25
Lipophilicity			
Log $P_{o/w}$ (iLOGP)	2.56	2.59	2.64
Log $P_{o/w}$ (XLOGP3)	1.63	2.05	2.31
Log $P_{o/w}$ (WLOGP)	1.80	2.16	1.91
Log $P_{o/w}$ (MLOGP)	0.83	1.63	1.49
Log $P_{o/w}$ (SILICOS-IT)	2.74	2.79	2.87
Consensus Log $P_{o/w}$	1.91	2.24	2.24
Water solubility			
Log *S* (ESOL)	−2.85	−3.07	−3.21
Solubility	4.02e-01 mg/mL; 1.42e-03 mol/L	2.18e-01 mg/mL; 8.43e-04 mol/L	1.56e-01 mg/mL; 6.11e-04 mol/L
Class	Soluble	Soluble	Soluble
Log *S* (Ali)	−2.40	−2.48	−2.75
Solubility	1.12e + 00 mg/mL; 3.94e-03 mol/L	8.55e-01 mg/mL; 3.30e-03 mol/L	4.52e-01 mg/mL; 1.77e-03 mol/L
Class	Soluble	Soluble	Soluble
Log *S* (SILICOS-IT)	−4.69	−4.64	−4.75
Solubility	5.82e-03 mg/mL; 2.06e-05 mol/L	5.97e-03 mg/mL; 2.30e-05 mol/L	4.57e-03 mg/mL; 1.79e-05 mol/L
Class	Moderately soluble	Moderately soluble	Moderately soluble
Pharmacokinetics			
GI absorption	High	High	High
BBB permeant	Yes	Yes	Yes
P-gp substrate	Yes	Yes	Yes
CYP1A2 inhibitor	Yes	Yes	Yes
CYP2C19 inhibitor	Yes	No	No
CYP2C9 inhibitor	No	No	No
CYP2D6 inhibitor	Yes	Yes	Yes
CYP3A4 inhibitor	Yes	Yes	Yes
Log K_p (skin permeation) cm/s	−6.87	−6.43	−6.22
Druglikeness			
Lipinski	Yes; 0 violation	Yes; 0 violation	Yes; 0 violation
Ghose	Yes	Yes	Yes
Veber	Yes	Yes	Yes
Egan	Yes	Yes	Yes
Muegge	Yes	Yes	Yes
Bioavailability Score	0.55	0.55	0.55
Medicinal chemistry			
PAINS	0 alert	0 alert	0 alert
Brenk	0 alert	0 alert	0 alert
Leadlikeness	Yes	Yes	Yes
Synthetic accessibility	2.33	2.25	2.39

substrate and Log K_p properties, which explore the blood–brain barrier permeability and drug-likeness of synthesized inhibitors. All the potent derivatives depicted increased gastrointestinal absorption and P-gp substrate ability that make the compounds safer and better feasible for drug candidacy. These derivatives also exhibited better efficacy and represented drug-likeness following various rules such as Ghose, Lipinski, Egan, Veber and Muegge, while bioavailability also showed good score to make them lead drug candidate. The results shown in Table 4 depict that the synthetic derivatives might be developed as possible drugs to treat Alzheimer's disease.

4. Conclusions

In summary, the current study reports the facile synthesis of pyrimidine-morpholine compounds. The target structures were characterized by spectroscopic techniques including FTIR, ^{1}H- and ^{13}C NMR. Compound **5e** was also characterized through X-ray crystallography. The use of various commercially accessible boronic acids presented an auspicious opportunity for the incorporation of structural diversity on the pyrimidine scaffold. The synthesized compounds were tested against acetylcholinesterase and butyrylcholinesterase enzymes. *In vitro* results revealed potent cholinesterase inhibition with preferable selectivity towards AChE. Compound **5h** was identified as the lead dual inhibitor with several folds strong inhibition profile than standard drugs whereas compounds **5a-g**, **5j** and **5l** were selective inhibitors of AChE. Kinetics studies revealed that the most efficacious inhibitor **5h** inhibits the AChE in a non-competitive manner. Molecular docking analysis depicted several vital contacts with amino acids in the binding cavity of both enzymes. Assessment of ADME parameters further supported the development of pyrimidine-morpholine compounds as promising leads towards the development of efficacious anti-Alzheimer's agents.

Declaration of Competing Interest

The authors declare that they have no known competing financial interests or personal relationships that could have appeared to influence the work reported in this paper.

Data availability

No data was used for the research described in the article.

Acknowledgments

The authors extend their appreciation to the Deanship of Scientific Research at King Khalid University for supporting this work through research groups program under grant number RGP.2/334/44.

Appendix A. Supplementary data

Supplementary data to this article can be found online at https://doi.org/10.1016/j.bioorg.2023.106868.

References

[1] A. Iraji, M. Khoshneviszadeh, O. Firuzi, M. Khoshneviszadeh, N. Edraki, Novel small molecule therapeutic agents for Alzheimer disease: Focusing on BACE1 and multi-target directed ligands, Bioorg. Chem. 97 (2020), 103649, https://doi.org/10.1016/j.bioorg.2020.103649.
[2] L. Minati, T. Edginton, M.G. Bruzzone, G. Giaccone, Current concepts in Alzheimer's disease: a multidisciplinary review, Am. J. Alzheimers Dis. Other Demen. 24 (2009) 95–121, https://doi.org/10.1177/1533317508328602.
[3] X. Du, X. Wang, M. Geng, Alzheimer's disease hypothesis and related therapies, Transl. Neurodegener. 7 (2018) 1–7, https://doi.org/10.1186/s40035-018-0107-y.
[4] J. Mottaghipisheh, H. Taghrir, A. Boveiri Dehsheikh, K. Zomorodian, C. Irajie, M. Mahmoodi Sourestani, A. Iraji, Linarin, a glycosylated flavonoid, with potential therapeutic attributes: A comprehensive review, Pharmaceuticals. 14 (2021) 1104, https://doi.org/10.3390/ph14111104.
[5] C.G. Ballard, N.H. Greig, A.L. Guillozet-Bongaarts, A. Enz, S. Darvesh, Cholinesterases: Roles in the brain during health and disease, Curr. Alzheimer Res. 2 (2005) 307–318, https://doi.org/10.2174/1567205054367838.
[6] A. Saeed, P.A. Mahesar, S. Zaib, M.S. Khan, A. Matin, M. Shahid, J. Iqbal, Synthesis, cytotoxicity and molecular modelling studies of new phenylcinnamide derivatives as potent inhibitors of cholinesterases, Eur. J. Med. Chem. 78 (2014) 43–53, https://doi.org/10.1016/j.ejmech.2014.03.015.
[7] M.B. Colović, D.Z. Krstić, T.D. Lazarević-Pašti, A.M. Bondžić, V.M. Vasić, Acetylcholinesterase inhibitors: Pharmacology and toxicology, Curr. Neuropharmacol. 11 (2013) 315–335, https://doi.org/10.2174/1570159X11311030006.
[8] G.T. Grossberg, Cholinesterase inhibitors for the treatment of Alzheimer's disease: Getting on and staying on, Curr. Ther. Res. Clin. Exp. 64 (2003) 216–235, https://doi.org/10.1016/S0011-393X(03)00059-6.
[9] H. Pourtaher, A. Hasaninejad, A. Iraji, Design, synthesis, in silico and biological evaluations of novel polysubstituted pyrroles as selective acetylcholinesterase inhibitors against Alzheimer's disease, Sci. Rep. 12 (2022) 15236, https://doi.org/10.1038/s41598-022-18224-6.
[10] J. Lalut, H. Payan, A. Davis, C. Lecoutey, R. Legay, J. Sopkova-de Oliveira Santos, S. Claeysen, P. Dallemagne, C. Rochais, Rational design of novel benzisoxazole derivatives with acetylcholinesterase inhibitory and serotoninergic 5-HT4 receptors activities for the treatment of Alzheimer's disease, Sci. Rep. 10 (2020) 3014, https://doi.org/10.1038/s41598-020-59805-7.
[11] Y. Pourshojaei, A. Abiri, K. Eskandari, Z. Haghighijoo, N. Edraki, A. Asadipour, Phenoxyethyl Piperidine/Morpholine Derivatives as PAS and CAS Inhibitors of Cholinesterases: Insights for Future Drug Design, Sci. Rep. 9 (2019) 19855, https://doi.org/10.1038/s41598-019-56463-2.
[12] S. Pant, A. Kapri, S. Nain, Pyrimidine analogues for the management of neurodegenerative diseases, Eur. J. Med. Chem. Rep. 6 (2022), 100095, https://doi.org/10.1016/j.ejmcr.2022.100095.
[13] M. Bortolami, F. Pandolfi, V. Tudino, A. Messore, V.N. Madia, D. De Vita, R. Di Santo, R. Costi, I. Romeo, S. Alcaro, M. Colone, A. Stringaro, A. Espargaró, R. Sabatè, L. Scipione, New Pyrimidine and Pyridine Derivatives as Multitarget Cholinesterase Inhibitors: Design, Synthesis, and *In Vitro* and In Cellulo Evaluation, ACS Chem. Nerosci. 12 (2021) 4090–4112, https://doi.org/10.1021/acschemneuro.1c00485.
[14] B. Dubois, H.H. Feldman, C. Jacova, J.L. Cummings, S.T. Dekosky, P. Barberger-Gateau, Revising the definition of Alzheimer's disease: A new lexicon, Lancet Neurol. 9 (2010) 1118–1127, https://doi.org/10.1016/S1474-4422(10)70223-4.
[15] P.S. Aisen, S. Andrieu, C. Sampaio, M. Carrillo, Z.S. Khachaturian, B. Dubois, Report of the task force on designing clinical trials in early (predementia) AD, Neurology 76 (2011) 280–286, https://doi.org/10.1212/WNL.0b013e318207b1b9.
[16] B. Dubois, H. Hampel, H.H. Feldman, P. Scheltens, P. Aisen, S. Andrieu, Preclinical Alzheimer's disease: Definition, natural history, and diagnostic criteria Alzheimer's & dementia, J. Alzheimer's Assoc. 12 (2016) 292–323, https://doi.org/10.1016/j.jalz.2016.02.002.
[17] E. Vitaku, D.T. Smith, J.T. Njardarson, Analysis of the Structural Diversity, Substitution Patterns, and Frequency of Nitrogen Heterocycles among U.S. FDA Approved Pharmaceuticals, J. Med. Chem. 57 (2014) 10257–10274, https://doi.org/10.1021/jm501100b.
[18] S. Nadar, T. Khan, Pyrimidine: An elite heterocyclic leitmotif in drug discovery-synthesis and biological activity, Chem. Biol. Drug Des. 100 (2022) 818–842, https://doi.org/10.1111/cbdd.14001.
[19] C.M. Bhalgat, M.I. Ali, B. Ramesh, G. Ramu, Novel pyrimidine and its triazole fused derivatives: synthesis and investigation of antioxidant and anti-inflammatory activity, Arab. J. Chem. 7 (2014) 986–993, https://doi.org/10.1016/j.arabjc.2010.12.021.
[20] Y.Y. Huang, L.Y. Wang, C.H. Chang, Y.H. Kuo, K. Kaneko, H. Takayama, M. Kimura, S.H. Juang, F.F. Wong, One-pot synthesis and antiproliferative evaluation of pyrazolo[3,4-d]pyrimidine derivatives, Tetrahedron 68 (2012) 9658–9664, https://doi.org/10.1016/j.tet.2012.09.054.
[21] Y. Liu, R. Laufer, N.K. Patel, G. Ng, P.B. Sampson, S.W. Li, Y. Lang, M. Feher, R. Brokx, I. Beletskaya, R. Hodgson, Discovery of Pyrazolo[1,5 a]pyrimidine TTK Inhibitors: CFI-402257 is a Potent, Selective, Bioavailable Anticancer Agent, ACS Med. Chem. Lett. 7 (2016) 671–675, https://doi.org/10.1021/acsmedchemlett.5b00485.
[22] A.P. Kourounakis, D. Xanthopoulos, A. Tzara, Morpholine as a privileged structure: a review on the medicinal chemistry and pharmacological activity of morpholine containing bioactive molecules, Med. Res. Rev. 40 (2020) 709–752, https://doi.org/10.1002/med.21634.
[23] A. Kumari, R.K. Singh, Morpholine as ubiquitous pharmacophore in medicinal chemistry: Deep insight into the structure-activity relationship (SAR), Bioorg. Chem. 96 (2020), 103578, https://doi.org/10.1016/j.bioorg.2020.103578.
[24] M. Al-Ghorbani, B. Begum, A. Zabiulla, S.V. Mamatha, S.A. Khanum, Piperazine and morpholine: synthetic preview and pharmaceutical applications, J. Chem. Pharm. Res. 7 (2015) 281–301, https://doi.org/10.5958/0974-360X.2015.00100.6.
[25] M.J. Naim, O. Alam, M.J. Alam, P. Alam, N. Shrivastava, A review on pharmacological profile of Morpholine derivatives, Int. J. Pharmacol. Pharm. Sci. 3 (2015) 40–51.
[26] R. Kumar, R.V. Srinivasa, S. Kapur, Emphasizing morpholine and its derivatives (Maid): typical candidate of pharmaceutical importance, Int. J. Chem. Sc. 14 (2016) 1777–1788.
[27] F. Arshad, M.F. Khan, W. Akhtar, M.M. Alam, L.M. Nainwal, S.K. Kaushik, M. Akhter, S. Parvez, S.M. Hasan, M. Shaquiquzzaman, Revealing quinquennial journey of morpholine: a SAR based review, Eur. J. Med. Chem. 167 (2019) 324–356, https://doi.org/10.1016/j.ejmech.2019.02.015.
[28] J. Hassan, M. Sévignon, C. Gozzi, E. Schulz, M. Lemaire, Aryl−aryl bond formation one century after the discovery of the Ullmann reaction, Chem. Rev. 102 (2002) 1359–1470, https://doi.org/10.1021/cr000664r.
[29] X.Y. Dong, Y.F. Zhang, C.L. Ma, Q.S. Gu, F.L. Wang, Z.L. Li, S.P. Jiang, X.Y. Liu, A general asymmetric copper-catalysed Sonogashira C (sp 3)–C (sp) coupling, Nat. Chem. 11 (2019) 1158–1166, https://doi.org/10.1038/s41557-019-0346-2.
[30] C.S. Yeung, V.M. Dong, Catalytic dehydrogenative cross-coupling: forming carbon-carbon bonds by oxidizing two carbon-hydrogen bonds, Chem. Rev. 111 (2011) 1215, https://doi.org/10.1021/cr100280d.
[31] S.H. Leenders, R. Gramage-Doria, B. de Bruin, J.N. Reek, Transition metal catalysis in confined spaces, Chem. Soc. Rev. 44 (2015) 433, https://doi.org/10.1039/c4cs00192c.
[32] J. Choi, G.C. Fu, Transition metal-catalyzed alkyl-alkyl bond formation: Another dimension in cross-coupling chemistry, Science 356 (2017) 6334, https://doi.org/10.1126/science.aaf7230.
[33] K. Muto, J. Yamaguchi, D.G. Musaev, K. Itami, Decarbonylative organoboron cross-coupling of esters by nickel catalysis, Nat. Commun. 6 (2015) 7508, https://doi.org/10.1038/ncomms8508.
[34] Y. Li, Y. Luo, L. Peng, Y. Li, B. Zhao, W. Wang, H. Pang, Y. Deng, R. Bai, Y. Lan, G. Yin, Reaction scope and mechanistic insights of nickel-catalyzed migratory Suzuki-Miyaura cross-coupling, Nat. Commun. 11 (2020) 417, https://doi.org/10.1038/s41467-019-14016-1.
[35] N. Hazari, P.R. Melvin, M.M. Beromi, Well-defined nickel and palladium precatalysts for cross-coupling, Nat. Rev. Chem. 1 (2017) 0025, https://doi.org/10.1038/s41570-017-0025.
[36] L. Guo, W. Srimontree, C. Zhu, B. Maity, X. Liu, L. Cavallo, M. Rueping, Nickel-catalyzed Suzuki-Miyaura cross-couplings of aldehydes, Nat. Commun. 10 (2019) 1957, https://doi.org/10.1038/s41467-019-09766-x.
[37] T.N. Ye, Y. Lu, Z. Xiao, J. Li, T. Nakao, H. Abe, Y. Niwa, M. Kitano, T. Tada, H. Hosono, Palladium-bearing intermetallic electride as an efficient and stable catalyst for Suzuki cross-coupling reactions, Nat. Commun. 10 (2019) 5653, https://doi.org/10.1038/s41467-019-13679-0.
[38] F.X. Felpin, S. Sengupta, Biaryl synthesis with arenediazonium salts: cross-coupling, CH-arylation and annulation reactions, Chem. Soc. Rev. 48 (2019) 1150–1193, https://doi.org/10.1039/c8cs00453f.
[39] N. Miyaura, A. Suzuki, Palladium-catalyzed cross-coupling reactions of organoboron compounds, Chem. Rev. 95 (1995) 2457–2483, https://doi.org/10.1021/cr00039a007.
[40] J. Sherwood, J.H. Clark, I.J. Fairlamb, J.M. Slattery, Solvent effects in palladium catalysed cross-coupling reactions, Green Chem. 21 (2019) 2164–2213, https://doi.org/10.1039/C9GC00617F.
[41] S.E. Hooshmand, B. Heidari, R. Sedghi, R.S. Varma, Recent advances in the Suzuki-Miyaura cross-coupling reaction using efficient catalysts in eco-friendly media, Green Chem. 21 (2019) 381–405, https://doi.org/10.1039/C8GC02860E.
[42] J. Magano, J.R. Dunetz, Large-scale applications of transition metal-catalyzed couplings for the synthesis of pharmaceuticals, Chem. Rev. 111 (2011) 2177–2250, https://doi.org/10.1021/cr100346g.
[43] E. Negishi, Magical power of transition metals: past, present, and future, Angew. Chem. Int. Ed. 50 (2011) 6738–6764, https://doi.org/10.1002/anie.201101380.

[44] C. Torborg, M. Beller, Recent applications of palladium-catalyzed coupling reactions in the pharmaceutical, agrochemical, and fine chemical industries, Adv. Synth. Catal. 351 (2009) 3027–3043, https://doi.org/10.1002/adsc.200900587.
[45] M.F. Lipton, M.A. Mauragis, M.T. Maloney, M.F. Veley, D.W. VanderBor, J. J. Newby, R.B. Appell, E.D. Daugs, The synthesis of OSU 6162: efficient, large-scale implementation of a Suzuki coupling, Org. Process Res. Dev. 7 (2003) 385–392, https://doi.org/10.1021/op025620u.
[46] D.A. Conlon, A. Drahus-Paone, G.J. Ho, B. Pipik, R. Helmy, J.M. McNamara, Y. J. Shi, J.M. Williams, D. Macdonald, D. Deschênes, M. Gallant, Process development and large-scale synthesis of a PDE4 inhibitor, Org. Process Res. Dev. 10 (2006) 36–45, https://doi.org/10.1021/op050116l.
[47] H. Doucet, J.C. Hierso, Palladium coupling catalysts for pharmaceutical applications, Curr. Opin. Drug Discov. Devel. 10 (2007) 672–690.
[48] S.D. Roughley, A.M. Jordan, The medicinal chemist's toolbox: an analysis of reactions used in the pursuit of drug candidates, J. Med. Chem. 54 (2011) 3451–3479, https://doi.org/10.1021/jm200187y.
[49] I. Khan, A. Ibrar, S. Zaib, S. Ahmad, N. Furtmann, S. Hameed, J. Simpson, J. Bajorath, J. Iqbal, Active compounds from a diverse library of triazolothiadiazole and triazolothiadiazine scaffolds: synthesis, crystal structure determination, cytotoxicity, cholinesterase inhibitory activity, and binding mode analysis, Bioorg. Med. Chem. 22 (2014) 6163–6173, https://doi.org/10.1016/j.bmc.2014.08.026.
[50] I. Khan, S. Zaib, A. Ibrar, N.H. Rama, J. Simpson, J. Iqbal, Synthesis, crystal structure and biological evaluation of some novel 1, 2, 4-triazolo [3, 4-b]-1, 3, 4-thiadiazoles and 1, 2, 4-triazolo [3, 4-b]-1, 3, 4-thiadiazines, Eur. J. Med. Chem. 78 (2014) 167–177, https://doi.org/10.1016/j.ejmech.2014.03.046.
[51] I. Khan, S.M. Bakht, A. Ibrar, S. Abbas, S. Hameed, J.M. White, U.A. Rana, S. Zaib, M. Shahid, J. Iqbal, Exploration of a library of triazolothiadiazole and triazolothiadiazine compounds as a highly potent and selective family of cholinesterase and monoamine oxidase inhibitors: design, synthesis, X-ray diffraction analysis and molecular docking studies, RSC Adv. 5 (2015) 21249–21267, https://doi.org/10.1039/C5RA00906E.
[52] A. Ibrar, A. Khan, M. Ali, R. Sarwar, S. Mehsud, U. Farooq, S.M. Halimi, I. Khan, A. Al-Harrasi, Combined in vitro and in silico studies for the anticholinesterase activity and pharmacokinetics of coumarinyl thiazoles and oxadiazoles, Front. Chem. 6 (2018) 61, https://doi.org/10.3389/fchem.2018.00061.
[53] S.A. Shehzadi, I. Khan, A. Saeed, F.A. Larik, P.A. Channar, M. Hassan, H. Raza, Q. Abbas, S.Y. Seo, One-pot four-component synthesis of thiazolidin-2-imines using CuI/ZnII dual catalysis: A new class of acetylcholinesterase inhibitors, Bioorg. Chem. 84 (2019) 518–528, https://doi.org/10.1016/j.bioorg.2018.12.002.
[54] S. Zaib, R. Munir, M.T. Younas, N. Kausar, A. Ibrar, S. Aqsa, N. Shahid, T.T. Asif, H. O. Alsaab, I. Khan, Hybrid Quinoline-Thiosemicarbazone Therapeutics as a New Treatment Opportunity for Alzheimer's Disease-Synthesis, In Vitro Cholinesterase Inhibitory Potential and Computational Modeling Analysis, Molecules 26 (2021) 6573, https://doi.org/10.3390/molecules26216573.
[55] R. Munir, M. Zia-ur-Rehman, S. Murtaza, S. Zaib, N. Javid, S.J. Awan, K. Iftikhar, M.M. Athar, I. Khan, Microwave-Assisted Synthesis of (Piperidin-1-yl)quinolin-3-yl)methylene)hydrazinecarbothioamides as Potent Inhibitors of Cholinesterases: A Biochemical and In Silico Approach, Molecules 26 (2021) 656, https://doi.org/10.3390/molecules26030656.
[56] M.Y. Ali, S. Zaib, S. Jannat, I. Khan, Discovery of potent and selective dual cholinesterases and β-secretase inhibitors in pomegranate as a treatment for Alzheimer's disease, Bioorg. Chem. 129 (2022), 106137, https://doi.org/10.1016/j.bioorg.2022.106137.
[57] J.L. Woodring, K.A. Bachovchin, K.G. Brady, M.F. Gallerstein, J. Erath, S. Tanghe, S.E. Leed, A. Rodriguez, K. Mensa-Wilmot, R.J. Sciotti, M.P. Pollastri, Optimization of physicochemical properties for 4-anilinoquinazoline inhibitors of trypanosome proliferation, Eur. J. Med. Chem. 141 (2017) 446–459, https://doi.org/10.1016/j.ejmech.2017.10.007.
[58] G.L. Ellman, K.D. Courtney, V. Andres, R.M. Featherstone, A new and rapid colorimetric determination of acetylcholinesterase activity, Biochem. Pharmacol. 7 (1961) 88–95, https://doi.org/10.1016/0006-2952(61)90145-9.
[59] F. Nachon, E. Carletti, C. Ronco, M. Trovaslet, Y. Nicolet, L. Jean, P.Y. Renard, Crystal structures of human cholinesterases in complex with huprine W and tacrine: Elements of specificity for anti-Alzheimer's drugs targeting acetyl- and butyrylcholinesterase, J. Biochem. 453 (2013) 393–399, https://doi.org/10.1042/BJ20130013.
[60] J. Iqbal, S. Zaib, A. Saeed, M. Muddassar, Biological evaluation of halogenated thioureas as cholinesterases inhibitors against Alzheimer's disease & molecular modeling studies, Lett. Drug Des. Discov. 12 (2015) 488–494, https://doi.org/10.2174/1570180812666141201222247.
[61] P.P. Labute, P. Protonate, 3D, Chemical Computing Group, 2007. Available online: http://www.chemcomp.com/journal/proton.htm (accessed on 10th September 2022).
[62] Chemical Computing Group's Molecular Operating Environment (MOE) MOE 2019. 0201 Available online: http://www.chemcomp.com/MOEMolecular_Operating_Environment.htm (accessed on 10th September 2022).
[63] LeadIT Version 2.3.2; BioSolveIT GmbH: Sankt Augustin, Germany, 2017. Available online: www.biosolveit.de/LeadIT (accessed on 10th September 2022).
[64] N. Schneider, G. Lange, S. Hindle, R. Klein, M. Rarey, A consistent description of hydrogen bond and dehydration energies in protein-ligand complexes: Methods behind the HYDE scoring function, J. Comput. Aided Mol. Des. 27 (2013) 15–29, https://doi.org/10.1007/s10822-012-9626-2.
[65] BIOVIA Discovery Studio Client v19.1.0.18287. Accelrys Discovery Studio; Accelrys Software Inc.: San Diego, CA, USA, 2019 (accessed on 10th September 2022).
[66] J.C. Gordon, J.B. Myers, T. Folta, V. Shoja, L.S. Heath, A. Onufriev, H++: a server for estimating pKas and adding missing hydrogens to macromolecules, Nucleic Acids Res. 33 (2005) 368–371, https://doi.org/10.1093/nar/gki464.
[67] D.A. Case, K. Belfon, I.Y. Ben-Shalom, S.R. Brozell, D.S. Cerutti, T.E. Cheatham, V. C. III, T.A. Darden, R.E. Duke, G. Giambasu, M.K. Gilson, AMBER2020, university of California, San Fransisco. J. Amer. Chem. Soc. 142 (2020) 3823-3835. https://www.researchgate.net/publication/233420507.
[68] J.A. Maier, C. Martinez, K. Kasavajhala, L. Wickstrom, K.E. Hauser, C. Simmerling, ff14SB: Improving the Accuracy of Protein Side Chain and Backbone Parameters from ff99SB, J. Chem. Theory Comput. 11 (2015) 3696–3713, https://doi.org/10.1021/acs.jctc.5b00255.
[69] J. Träg, D. Zahn, Improved GAFF2 parameters for fluorinated alkanes and mixed hydro and fluorocarbons, J. Mol. Model. 25 (2019) 39, https://doi.org/10.1007/s00894-018-3911-5.
[70] J. Wang, W. Wang, P.A. Kollman, D.A. Case, Automatic atom type and bond type perception in molecular mechanical calculations, J. Mol. Graph. Model. 25 (2006) 247–260, https://doi.org/10.1016/j.jmgm.2005.12.005.
[71] W.L. Jorgensen, J. Chandrasekhar, J.D. Madura, R.W. Impey, M.L. Klein, Comparison of simple potential functions for simulating liquid water, J. Chem. Phys. 79 (1983) 926–935, https://doi.org/10.1063/1.445869.
[72] I.S. Joung, T.E. Cheatham, Determination of Alkali and Halide Monovalent Ion Parameters for Use in Explicitly Solvated Biomolecular Simulations, J. Phys. Chem. B 112 (2008) 9020–9041, https://doi.org/10.1021/jp8001614.
[73] R.J. Loncharich, B.R. Brooks, R.W. Pastor, Langevin dynamics of peptides: the frictional dependence of isomerization rates of N-acetylalanyl-N'-methylamide, Biopolymers 32 (1992) 523–535, https://doi.org/10.1002/bip.360320508.
[74] Y. Lin, D. Pan, J. Li, L. Zhang, X. Shao, Application of Berendsen barostat in dissipative particle dynamics for nonequilibrium dynamic simulation, J. Chem. Phys. 146 (2017), 124108, https://doi.org/10.1063/1.4978807.
[75] D.R. Roe, T.E. Cheatham, PTRAJ and CPPTRAJ: Software for Processing and Analysis of Molecular Dynamics Trajectory Data, J. Chem. Theory Comput. 9 (2013) 3084–3095, https://doi.org/10.1021/ct400341p.
[76] W. Humphrey, A. Dalke, K. Schulten, VMD: Visual molecular dynamics, J. Mol. Graph. 14 (1996) 33–38, https://doi.org/10.1016/0263-7855(96)00018-5.
[77] A. Daina, O. Michielin, V. Zoete, SwissADME: A free web tool to evaluate pharmacokinetics, drug-likeness and medicinal chemistry friendliness of small molecules, Sci. Rep. 7 (2017) 42717, https://doi.org/10.1038/srep42717.
[78] A. Daina, O. Michielin, V. Zoete, iLOGP: A simple, robust, and efficient description of n-octanol/water partition coefficient for drug design using the GB/SA approach, J. Chem. Inf. Model. 54 (2014) 3284–3301, https://doi.org/10.1021/ci500467k.
[79] A. Daina, V. Zoete, A BOILED-Egg to predict gastrointestinal absorption and brain penetration of small molecules, ChemMedChem 11 (2016) 1117–1121, https://doi.org/10.1002/cmdc.201600182.
[80] I. Khan, A. Khan, S.A. Halim, M. Khan, S. Zaib, B. Essa, M. Al-Yahyaei, A. Al-Harrasi, A. Ibrar, Utilization of the common functional groups in bioactive molecules: Exploring dual inhibitory potential and computational analysis of keto esters against α-glucosidase and carbonic anhydrase-II enzymes, Int. J. Biol. Macromol. 167 (2021) 233–244, https://doi.org/10.1016/j.ijbiomac.2020.11.170.
[81] P. Ertl, B. Rohde, B.P. Selzer, Fast calculation of molecular polar surface area as a sum of fragment-based contributions and its application to the prediction of drug transport properties, J. Med. Chem. 43 (2000) 3714–3717, https://doi.org/10.1021/jm000942e.